Wag31, a membrane tether, is crucial for lipid homeostasis in mycobacteria

Yogita Kapoor[1,2], Himani Khurana[3#], Debatri Dutta[1#], Arnab Chakraborty[3], Anshu Priya[2,4], Archana Singh[2,4], Siddhesh S. Kamat[3], Neeraj Dhar,[5,6,] Thomas J. Pucadyil[3], Vinay Kumar Nandicoori[1,2,7]

1. CSIR-Centre for Cellular and Molecular Biology (CSIR-CCMB), Hyderabad, 500007
2. AcSIR, Ghaziabad-201002
3. Indian Institute of Science Education and Research, Pune, 411008
4. CSIR-Institute of Genomics and Integrative Biology (CSIR-IGIB), New Delhi, 110025
5. Vaccine and Infectious Disease Organisation, University of Saskatchewan, Canada, S7N 5E3
6. Department of Biochemistry, Microbiology and Immunology, University of Saskatchewan, Canada S7N 5E5
7. National Institute of Immunology, New Delhi 110067

# contributed equally to this work

Address correspondence to vinaykn@ccmb.res.in, vinaykn@nii.ac.in

Keywords: Wag31, intracellular lipid inclusions (ILIs), lipid homeostasis, membrane-tether

Abstract

The mycobacterial cytoskeletal protein Wag31 is necessary for maintaining cell shape and directing cellular growth and elongation. Wag31 has a characteristic N-terminal DivIVA-domain and a C-terminal coiled-coil domain. While the role of Wag31 in polar elongation is known, there is limited mechanistic insight on how it orchestrates growth and elongation. In this report, we delineate roles of the N- and C-terminal domains of Wag31 using genetics, state-of-the-art multi-omics, biochemical, and imaging approaches. We show that Wag31 predominantly interacts with several membrane-associated proteins involved in lipid metabolism, cell wall synthesis and division. Native levels of Wag31 are critical for the maintenance and distribution of membrane lipids. Both depletion and overexpression of Wag31 perturbs lipid homeostasis, leading to the formation of intracellular lipid inclusions (ILIs). Protein-lipid crosslinking and imaging studies reveal that purified Wag31 can bind and effectively tether Cardiolipin (CL)-containing liposomes. We further show that the tethering activity lies in the DivIVA-domain containing N-terminal of Wag31 while the C-terminal mediates protein-protein interactions of Wag31. Despite retaining its ability to interact with partner proteins, the DivIVA domain-deleted Wag31 mutant shows defects in liposome tethering *in vitro* and non-polar localization of CL *in vivo*, which eventually causes lethality. Our study suggests that membrane tethering 'licenses' Wag31 to form scaffolds that help orchestrate protein-lipid and protein-protein interactions necessary for mycobacterial growth and survival.

Introduction

Cell division is a critical event in the life of a bacterium as it is the prime mode of bacterial growth and reproduction. Hence, the process of their division is tightly knitted. The key process in bacterial cell division, i.e., assembly of the FtsZ ring at the mid-cell (1), is tightly regulated by the Min and Nucleoid occlusion systems (2-6). Mycobacterium, which comprises clinically relevant pathogens- *Mycobacterium tuberculosis (Mtb)*, *Mycobacterium leprae,* and *Mycobacterium abscessus* lacks both the regulators of FtsZ ring placement (7). Instead, they encode for a DivIVA protein, usually encoded by Firmicutes and other Actinobacteria (8-11). It is necessary that the bacterial shape, crucial for normal cellular physiology, is maintained during cell division. Rod-shaped bacteria such as *Escherichia coli* and *Bacillus subtilis* encode MreB and multiple MreB-like proteins that sustain the rod morphology of cells (12). *Mycobacterial spp*. lack MreB homologs (13, 14). The DivIVA protein of *Mtb* called Wag31 is known to regulate both cellular growth and morphology (10, 15), which makes it an exciting candidate to investigate.

DivIVA proteins were discovered three decades ago during the study of cell division mutants of *B. subtilis* (16). DivIVA proteins are rich in coiled-coil domains (17-21), which enable them to form higher oligomeric structures and, hence, scaffolds, making them suitable adaptor proteins (22, 23). They are known to play diverse roles in various species (24), e.g., they play dual roles of septum positioning and chromosome partitioning in *B. subtilis* (9, 25); cell-separation/resolution post-cell-division in *Listeria monocytogenes* (26, 27); pole formation and maturation in *Streptococcus spp*. (Fadda, 2007) In *Mycobacterium spp.*, Wag31 is an essential protein that senses negative membrane curvature found at poles and septum and localizes there (28). It plays roles in cellular elongation and septation in concert with other divisome and elongasome components (10, 15, 29). It is specifically found in higher amounts at the old pole, where it directs polar elongation by recruiting the acyl CoA carboxylase (ACCase) complex involved in fatty acid, mycolic acid, and methyl-branched chain lipid precursor synthesis (28, 30-32). It localizes to the septum after cytokinesis is over, perhaps for septal synthesis via its interactions with FtsI (32-34), though the process remains largely unknown. Consequently, loss of Wag31 leads to cell division defects- loss of polar elongation, which renders the cells 'round' in shape that occurs due to affected peptidoglycan (PG) synthesis (10, 15, 28). Though Wag31 participates in coordinating PG metabolism, the mechanism or the protein network by which it does so remains unknown.

Wag31 has also been associated with the maintenance of the intracellular membrane domain (IMD), a specialized compartment for lipid synthesis, localized predominantly at the old pole in consonance with pole elongation and spottily all around the plasma membrane where it may function to repair membrane defects (35-37). The loss of Wag31 leads to the delocalization of IMD and its protein markers, such as MurG and GlfT2, but it is not understood whether Wag31 plays a direct role in membrane-partitioning or it is just a consequence of localized membrane synthesis (34, 37). The role of Wag31in PG and lipid synthesis that drives cell division remains unclear. Despite numerous studies, the details of how Wag31 orchestrates mega-complexes at the pole or partitions the membrane into two to govern cellular elongation remain elusive.

Here, we endeavoured to address the lacunae in the functionality of Wag31 by asking the following questions- i) what are the ultrastructural changes that occur in mycobacteria due to the absence of Wag31, ii) do Wag31 deficient cells undergo transcriptional rewiring to adjust to cell division defects, iii) is the change in cellular morphology from ‘rod-to-round’ accompanied by altered lipid levels, iv) what is the interactome of Wag31, v) what are the functions of its N and C-terminal domains and finally vi) what is its relationship with the mycobacterial membrane. The present study shows that Wag31 levels are critical for maintaining lipid homeostasis in mycobacteria. Our results demonstrate that the N- and C-terminals of Wag31 have distinct functions. The N-terminal of Wag31 binds and tethers the membrane together while the C-terminal interacts with various proteins. Together, the domains help Wag31 to orchestrate membrane-localized processes essential for maintaining normal cellular morphology and physiology.

Results

Loss of Wag31 leads to the formation of intracellular lipid inclusions (ILIs)

In the pursuit of bridging the knowledge gap existing in the functionality of Wag31 (Fig. 1a), we generated a *Wag31* conditional mutant in *Msm*, by integrating a copy of *wag31* under tetracycline (ATc-tet off) regulation at the L5 locus and replacing the native copy with a hygromycin cassette (Fig. S1a). The mutant, *Δwag31*, thus generated, was confirmed by PCRs (Fig. S1b) and Western blotting (Fig. 1b). The lack of Wag31 led to a drop in the turbidity of culture (Fig. 1c). Analysis of bacillary survival *in vitro* by enumerating CFUs 12h post-ATc addition, revealed a 2 log fold difference in the survival of *Δwag31* (Fig. 1d). Given the essential role of Wag31 in causing polar growth of the cell, we investigated the effect of depletion of Wag31 on bacterial cellular morphology using electron microscopy (EM). Scanning EM (SEM) suggested that the absence of Wag31 caused a transition in the morphology of the cells from rod to round, as previously documented (10, 15, 38). Apart from round morphology (~36 %), we also observed a rod-to-round transformation stage in which cells were bulged at one pole with the other pole intact (Fig. 1e-g). To obtain detailed insights, we performed transmission EM (TEM), which divulges information on the internal structure of cells. We discovered spherical, electron-lucent bodies (indicated by an arrowhead in Fig.1h) in the cytosol of all the samples. While *Msm* and *Δwag31*-ATc harbored a few (~2-3) electron-lucent bodies, their numbers were drastically higher in the case of *Δwag31*+ATc (Fig. 1h). The cytosol of *Δwag31*+ATc was filled with multiple variable-sized bodies which resembled Lipid bodies that *Mycobacterium tuberculosis* (*Mtb)* accumulates inside the host (39, 40). As the term 'lipid bodies/lipid droplets' is used specifically for the lipids acquired by *Mtb* from the host cell, we referred to them as intracellular lipid inclusions (ILIs). We categorized the cells based on the number of ILIs they contained. Their distribution remained reasonably similar within *Msm* and *Δwag31*-ATc cells for all the classes (Fig. 1i). Whereas *Δwag31* treated with ATc had as high as 85% cells harboring more than 5 ILIs and very few cells with less than 5 ILIs (Fig. 1i). Our data, therefore, reports a novel observation of lipid accumulation when Wag31 is depleted from mycobacteria.

Wag31 levels influence lipid homeostasis

Next, we set out to analyze if the ILIs are indeed lipidic in nature by staining cells with BODIPY (493/503), a dye that preferentially partitions into neutral lipid droplets (41, 42). We stained either untreated or ATc-treated *Msm* and *Δwag31* with BODIPY and visualized them on a microscope. ATc-treated *Δwag31* cells displayed the highest level of BODIPY fluorescence, indicating the maximum abundance of lipid bodies among the three strains (Fig. 2a, c). Further, we examined whether the appearance of ILIs is associated just with the loss of Wag31 or is a consequence of deviations from the native expression level of Wag31. Towards this, we overexpressed Wag31 episomally using an isovaleronitrile (IVN) inducible system (*Msm::wag31*) (Fig. S2a) and stained the cells with BODIPY. Unlike Wag31 depletion, which resulted in spherical cells (Fig. 1e), Wag31 overexpression resulted in the bulging of cells from one pole (Fig. 2b). Additionally, the overexpression of Wag31 also led to lipid aggregates in the cell with a few larger 'donut-like' aggregates in the bulged pole (Fig 2b,d).

Lipid accumulation in both cases led us to inspect whether lipid metabolism is closely tied to Wag31 expression levels in mycobacteria. To investigate that possibility, total cellular lipids were extracted from *Msm,* Wag31 depletion, and overexpression conditions and subjected to semi-

quantitative LC-MS analysis (illustrated in Fig. 2e). Lipidomic analysis of *Δwag31*+ATc revealed an imbalance in the levels of neutral lipids, phospholipids, and free fatty acids in comparison to *Msm*-ATc (Fig. 2f-g). *Δwag31*+ATc cells had a significant accumulation of unsaturated diacylglycerols (~3-5 fold) and a very long chain containing (>C36) phosphatidylethanolamines (~5-32 fold). This was accompanied by increased levels of different chain lengths (C18-C24) of free fatty acids (~1.7-4 fold) and reduced levels of cardiolipins C70:0 & C70:1 (~3 fold). Wag31 overexpression, on the other hand, led to a 2-fold increase in the level of different species of alpha-mycolic acids (C74-C78) as compared to *Msm*+IVN (Fig. 2h), while other tested lipids remained unchanged (Fig. S2). Altogether, the results presented above demonstrate that Wag31 levels are crucial for maintaining lipid homeostasis in mycobacteria, the depletion and overexpression of which impact lipid metabolism differently.

Molecular interactions of Wag31 with membrane-associated proteins govern cellular homeostasis.

We reasoned that Wag31, an adaptor protein, might maintain lipid homeostasis by interacting with proteins involved in these pathways. To examine the protein interaction network of Wag31, we performed an interactome analysis by utilizing *Δwag31*, which expresses FLAG-Wag31 integrated at the L5 locus, and used FLAG-GFP as the control to differentiate from non-specific interactions. FLAG-Wag31 and FLAG-GFP from biological triplicates were immunoprecipitated using whole cell lysates from the log phase cells and subjected to mass spectrometry analysis (Fig. S3a & Table S2). This study identified both direct and indirect protein-partners of Wag31. The proteins identified were categorized based on their functions. It was found that Wag31 interacts with proteins involved in cell-wall elongation and division, lipid metabolism, intermediary metabolism and respiration and information pathways (translation, replication) (Fig. 3a, Fig. S4). Interactions of Wag31 with AccA3 and AccD5, subunits of the ACCase complex, and Rne or RNaseE (Msm4626), a membrane-associated protein, have been reported previously (28, 43). Subunits of ACCase complex and Rne were among the top 5 hits in our MS/MS data, validating our approach (Fig. 3a, marked with asterisk). The classification of the top 20 hits is represented in Fig. 3a. The highest number of protein interactors, expectedly, fell in the cell wall and cell processes category (Fig. 3a). For the present study, we focussed on the interactors found in the cell wall elongation and cell division and lipid metabolism functional categories to probe the cause behind the lipid dysbiosis phenotype.

MurG, involved in PG metabolism (36, 44-46), and SepIVA, involved in regulating septation and the spatial regulator of MurG (47) also surfaced in the interactome of Wag31. Msm1813, or acyl CoA carboxylase (ACAD), crucial for nascent fatty acid precursor synthesis, was also enriched in the interactome. Other lipid metabolism interactors of Wag31 included acyl-CoA dehydrogenase (Msm2080), involved in lipid catabolism; GpsA, involved in phospholipid biosynthesis; and Msm0372, involved in fatty acid biosynthesis. To validate the high-throughput data, we chose MurG, SepIVA and Msm2092 and performed pull-down assays with His-tagged Wag31. MmpL4 and MmpS5 which didn't appear in the interactome database were used as negative controls in this experiment. His-tagged Wag31 (Fig. 3b) was incubated with *Msm* lysates expressing 3X-FLAG tagged versions of the interactors and non-interactors mentioned above (Fig. 3c) and pulled-down with the help of cobalt beads followed by a western blot analysis. Results obtained confirmed the interaction of Wag31 with

MurG, SepIVA and Msm2092, but not with the MmpL4 and MmpS5, thus validating our data (Fig. 3d).

Since Wag31 is a spatiotemporal regulator of other proteins, we were intrigued to discover the localisation of its interacting partners. We used the data curated by Zhu et al. (48) and determined that Wag31 majorly interacts with membrane-associated proteins with a few exceptions (Fig. 3e, Fig. S3b). The mycobacterial plasma membrane has been recently shown to have a cell wall-associated compartment called PM-CW and a cell wall-free compartment called PM_f or IMD, which is the site for lipid synthesis. Based on the available data (36, 48, 49), we found that Wag31 interacts more with IMD-proteins than with PM-CW proteins (Fig. 3f.) In accordance with assigned roles (36), PM-CW residing proteins in the interactome are involved in cell wall and cell processes and intermediary metabolism and respiration. Similarly, IMD-homing proteins clustered in the lipid metabolism and cell wall synthesis category. These results suggest that Wag31 maintains lipid homeostasis and cellular morphology primarily through its interactions with the membrane proteins participating in such pathways.

Wag31 binds and tethers cardiolipin-containing membranes

Wag31 is a cytoplasmic protein that recognizes negative curvature regions in the cell, i.e., poles and septum (28). It also forms higher-order structural assemblies at the poles (21, 50). However, the precise mechanism by which Wag31 assemblies localize to the poles remains elusive. The predominant interactions of Wag31 with membrane-associated proteins (Fig. 3) were intriguing and led us to investigate if it can directly bind to membranes. We reasoned that such membrane binding activity might render it capable of acting as a scaffold that anchors and organizes other proteins, thereby modulating their functions. To test this, we performed a lipid crosslinking-based PLiMAP assay (Fig. 4a). Purified Wag31 was incubated with ~100 nm extruded liposomes containing each of the abundant classes of bacterial lipids phosphatidylethanolamine (PE), phosphatidylglycerol (PG), or cardiolipin (CL). Liposomes contained trace amounts of a reactive fluorescent lipid (RFL), which crosslinks with membrane-bound proteins upon photoactivation. These assays revealed that Wag31 preferentially binds CL- but not PG- or PE-containing liposomes (Fig. 4b). Both CL and PG are anionic lipids, and the preferential binding of Wag31 to CL indicates that the binding cannot be attributed to a charge-based interaction. Remarkably, the sensitive fluorescence-based detection revealed the presence of SDS-resistant higher-order oligomers of membrane-bound Wag31 (Fig. 4b).

Wag31 is a homolog of the DivIVA protein from *B. subtilis.* The latter has been shown to bind to the membrane via the N-terminal DivIVA domain (N-$DivIVA_{BS}$) (51). However, the functional significance of the N- & C- terminal domains of mycobacterial Wag31 has not been dissected. Considering that the Wag31 N-terminal region shares 42% sequence identity with N-$DivIVA_{BS}$ (50), we sought to inspect the effect of disruption of a particular residue (K20) in the N-terminus and the deletion of the entire N-terminus, encompassing the DivIVA domain (1-60 amino acids) on membrane binding (Fig. S5a). The K20 residue lies within a positively charged patch, which likely constitutes a membrane-associating surface in the intertwined loop region of Wag31(50). Moreover, mutating the K20 residue has been shown to decrease the cell length and elongation rate by 18% and 22%, respectively (34). The K20A mutation showed a marginal defect in binding to CL-liposomes (Fig. 4c-d), indicating that K20 alone is insufficient for membrane binding. However, $Wag31_{K20A}$ showed a marked defect in

forming SDS-resistant higher-order oligomers, as seen in the binding assays. Interestingly, deletion of the entire N-terminal domain caused a significant defect in both membrane binding and forming SDS-resistant higher-order oligomers (Fig. 4c-d). Surprisingly, binding was not entirely abolished, suggesting that the C-terminus of Wag31 may also contribute to membrane binding. Taken together, our results indicate that Wag31 preferentially binds CL-containing membranes and that regions other than the N-terminal domain contribute to membrane binding. The latter feature distinguishes Wag31 from $DivIVA_{BS}$, and Wag31 likely contains membrane binding sites located at both the N- and C-terminal regions, which might lead to differences in the manner in which it interacts with the membrane and partner proteins compared to $DivIVA_{BS}$.

To further confirm membrane binding, we imaged 100 nm-extruded CL-containing liposomes with a membrane dye DiI in the presence of Wag31. We used a GFP-tagged Wag31 mixed with an untagged Wag31 at a 1:10 molar ratio for these experiments. In the absence of Wag31-GFP, liposomes appeared as faint but distinct fluorescent puncta (Fig. 4e, first panel). Surprisingly, in reactions containing Wag31-GFP, we observed liposomes clustered into bright fluorescent puncta that were positive for Wag31-GFP (Fig. 4e, remaining panels). The Wag31 tetramer has been modelled as a long rod-shaped protein filament (21, 50) and such clustering of liposomes falls in congruence with the model. It indicates that these long filaments of Wag31 act to tether liposomes. We then systematically evaluated this effect by testing liposomes of different compositions and Wag31 mutants. Again, in the absence of Wag31, both PE- and CL-containing liposomes appeared as faint but distinct fluorescent puncta (Fig. 4f). The addition of Wag31 caused clustering of CL-containing liposomes into bright foci (Fig. 4f), which is quantified by a particle intensity analysis (Fig. 4g). This clustering was caused by membrane binding of Wag31 because PE-containing liposomes that do not bind Wag31 (Fig. 4b) showed no clustering (Fig. 4f,g). As expected, $Wag31_{\Delta N}$ was defective in membrane binding (Fig. 4c,d) and showed a severe tethering capacity defect (Fig. 4f,g). Surprisingly, $Wag31_{K20A}$, which showed a marginal defect in membrane binding (Fig. 4c,d), showed a marked defect in tethering capacity (Fig. 4f,g). Together, these results suggest that membrane-binding and membrane-tethering are non-overlapping attributes in the structure of Wag31, and the N-terminal DivIVA-domain is indispensable for membrane-tethering activity.

Tethering is crucial for the survival of mycobacteria

Results presented in Fig.4c indicate that Wag31 binds strongly to CL-containing membranes. CL is a negatively charged inverted cone-shaped lipid that has been shown to be concentrated at the sites of negative curvature in the bacterial cell, i.e., pole and septum (52, 53). Wag31 has been demonstrated previously to localize at sites of negative curvature (28). Their similar localization pattern, coupled with Wag31's affinity to bind to CL, led us to examine the effect of this binding *in vivo*. We hypothesized that modulations in Wag31 levels might alter CL distribution in the cell.

To examine this, we utilized a fluorophore 10-N-Nonyl-acridine orange (NAO) that is widely used to examine the localization of CL in prokaryotes and in the mitochondria of eukaryotes (52, 54, 55). NAO binds to anionic phospholipids with an affinity constant of 7×10^4 M^{-1} and to CL with an affinity constant of 2×10^6 M^{-1} (56). We stained *Msm and* Wag31 depleted and overexpressing cells with NAO and imaged them using a fluorescence microscope. While the localization pattern of NAO was polar in

Msm+ATc and *Δwag31*-ATc, there was a redistribution of red fluorescence to the cytosol and along the perimeter of the cell in *Δwag31*+ATc (Fig.5a-b). We quantified the distribution of fluorescence using a line profile which yielded peaks of intensity at the poles and a basal level of fluorescence along the lateral cell body for both *Msm*+ATc and *Δwag31*-ATc (Fig.5b). Wag31 overexpression also led to a change in the distribution of NAO from the poles and septum to 'donut-like' fluorescent foci in the cytosol (Fig.5c-d). As the affinity of NAO for CL is more than other anionic phospholipids and our result (shown in Fig. 4b) indicate that Wag31 prefers to bind CL over PG (another negatively charged phospholipid), the change in the distribution of NAO fluorescence implies that the loss or overexpression of Wag31 causes the mislocalization of CL in mycobacterium.

Subsequently, we investigated the impact of tethering-deficient Wag31 mutants on cell survival. Wag31 has an N-terminal domain joined to the C-terminal via a linker region. The N-terminal domain contains a positively charged patch in the intertwined region (the region between two helices in the N-terminus) and membrane binding has been attributed to this region (50). This patch is lined with conserved arginine and lysine residues, K15, K20, and R21 (50) (Fig. 5e). As our *in vitro* results suggest the importance of K20 and the DivIVA-domain in tethering, we performed complementation assays with the tethering-defective mutants to examine cell survival and morphology. *Δwag31* was complemented with an integrative copy of either Wag31 or $Wag31_{K20A}$ or $Wag31_{\Delta N}$. *Δwag31*+ATc showed a two log-fold difference in survival and a 40 % decrease in the percentage of rod-shaped cells compared with *Δwag31*-ATc (Fig. 5f-g). Complementation with Wag31 and $Wag31_{K20A}$ rescued the loss of cell viability and restored the rod shape of the cells (Fig. 5f-g), whereas $Wag31_{\Delta N}$ behaved similar to *Δwag31*+ATc. It neither restored the rod shape of the cells nor reversed the survival defect (Fig. 5f-g). These results highlight the importance of the N-terminal DivIVA-domain for sustaining mycobacterial morphology and survival.

Tethering is correlated to lipid levels and CL localization in mycobacteria

As described above, Wag31-mediated membrane tethering is an absolute for the survival of mycobacteria. Perturbations in lipid homeostasis and mislocalization of CL due to altered Wag31 levels hint at a correlation between its ability to function as a homotypic tether and maintain lipid composition and localization. To derive the mechanism behind it, we performed fluorescence imaging experiments with native and tethering defective mutants of Wag31. To investigate a role of tethering in lipid homeostasis in mycobacteria, we stained wildtype and complementation strains with BODIPY and quantified the fluorescence intensities. We observed comparable staining intensity in *Msm* +ATc and, *Δwag31* -ATc (Fig. 6a-b). *Δwag31*+ATc expectedly had the highest BODIPY staining intensity, indicating higher than normal lipid levels (Fig. 6a-b). Complementation with Wag31 fully restored the lipid levels to normal, whereas complementation with $Wag31_{K20A}$ couldn't restore the lipid levels completely (Fig. 6a-b). $Wag31_{\Delta N}$ exhibited higher lipid levels than *Δwag31*-ATc (Fig. 6a-b). These results highlight that the maintenance of lipid homeostasis by Wag31 is a consequence of its tethering activity.

Next, we examined the dependence of CL localisation on tethering by staining *Msm* +ATc, *Δwag31* -ATc, *Δwag31*+ATc, *Δwag31::wag31*+ATc, *Δwag31::wag31*$_{K20A}$+ATc, and *Δwag31:: wag31*$_{\Delta N}$ +ATc with NAO. NAO staining showed a polar and septal (in dividing cells) localization pattern in the

case of *Msm* and *Δwag31*-ATc, whereas it stained the cytosol and perimeter of the Wag31 depleted cells (Fig. 6c-d). Complementation with Wag31 restored NAO localization completely, whereas $Wag31_{K20A}$ restored it partially, which could be attributed to its limited tethering activity (Fig. 6c-d). Importantly, we observed a mis-localized pattern of NAO with $Wag31_{\Delta N}$ similar to Wag31 depletion (Fig. 6c-d). These results inform of the dependence of CL localization on membrane tethering activity of Wag31. Taken together, the data suggests the importance of the N-terminal region of Wag31 in regulating lipid homeostasis and localization.

The N and C-terminal domains of Wag31 have distinct functions.

Wag31 is a 272 amino-acids long protein that contains an N- and a C-terminal domain that are joined by a linker region (Fig. 7a). In this report, we established a role for the N-terminal region of Wag31 that comprises DivIVA-domain in membrane-tethering (Fig. 4). We also identified the protein-interaction network of Wag31 with the help of MS/MS analysis (Fig. 3 & Fig. S4). To investigate which domain of Wag31 promotes its interactions with other proteins, we generated *Msm* strains expressing either N-terminal ($Wag31_{\Delta N}$) or C-terminal truncated ($Wag31_{\Delta C}$) Wag31 (Fig. 7a) and performed a series of His pull-down experiments with both the mutants. To investigate the protein-binding ability of the domain truncation mutants, we tested them against novel interactors of Wag31 viz. MurG, SepIVA, and Msm2092 from our interactome database (Fig.3a) and AccA3, a known interactor of Wag31. MmpS5 served as a non-interactor negative control in the experiment.

We performed His pull-down assays utilizing *E. coli* lysates expressing either Wag31 or $Wag31_{\Delta C}$ or $Wag31_{\Delta N}$ (Fig. 7b, e). These lysates were mixed and incubated with *Msm* lysates expressing 3x-FLAG tagged versions of the above-mentioned proteins (Fig.7c, f) in separate reactions and subsequently pulled-down with Cobalt beads. The western blot analysis revealed that all the tested interactors bound to Wag31 (Fig. 7d, g). Expectedly, MmpS5, being a non-interactor of Wag31 did not bind to it (Fig. 7d). As shown in Fig. 7d, none of the interactors bound to $Wag31_{\Delta C}$, indicating that the presence of N-terminal DivIVA-domain is not sufficient to enable Wag31 to interact with other proteins. Interestingly, interactions with all the proteins were retained in the case of $Wag31_{\Delta N}$ (Fig. 7g), thus suggesting that Wag31 interacts with other proteins via its C-terminal. Taken together, the results suggest that the N-terminal region of Wag31 is involved in membrane-tethering through interactions with CL, and the C-terminal region is involved in modulating interactions with other membrane-associated proteins. Thus N-terminal and C-terminal of Wag31 have distinct molecular functions that together are crucial for maintaining cell shape, lipid homeostasis and survival of mycobacteria.

Discussion.

Wag31 modulates mycobacterial cell division by acting as an adaptor protein that recruits the elongation machinery to the old pole for unipolar growth of cells (10, 15, 28). In the absence of Wag31, rod-shaped cells advance into a spheroplast-like stage, which is thought to arise from dysregulated PG metabolism (10, 11, 28). Recently, Wag31 has been implicated in maintaining the lipid-rich IMD compartment (37). But the molecular mechanisms by which Wag31 manages these functions has remained unclear. In this study, we discover an additional function of Wag31 as a membrane tether,

which likely reconciles many of the previously ascribed functions of this protein into a unified model. To gain insights into defects associated with a change in cell shape, we imaged Wag31-deficient cells and found a dramatic accumulation of lipids in the form of ILIs. Interestingly, both *Msm* and *ΔWag31*-ATc showed the presence of ILIs, but in much less abundance, indicating that ILIs are a normal occurrence that may function to regulate cellular functions (Fig. 1g-h).

The loss of Wag31 leads to the accumulation of neutral lipids while its overexpression increase the levels of alpha-mycolic acids (α-MA), implying that the maintenance of native Wag31 levels is critical for the proper balance of lipid composition (Fig. 2f-h). The lipid classes that get impacted by the depletion of Wag31 vs overexpression are different. Wag31 is an adaptor protein that interacts with proteins of the ACCase complex (28, 30) that synthesize fatty acid precursors and regulate their activity (34). The varied response on lipid homeostasis could be attributed to a change in the stoichiometry of these interactions of Wag31. While Wag31 depletion would prevent such interactions from occurring and might affect lipid synthesis that directly depends on Wag31-protein partner interactions, its overexpression would lead to promiscuous interactions and a change in the stoichiometry of native interactions that would ultimately modulate lipid synthesis pathways.

A protein's interactome is akin to its functional fingerprint. Here, we identify 116 novel interacting partners of Wag31 through mass spectrometry and validate three of these interactions, namely with MurG, SepIVA and Msm2092, through pull-down studies (Fig. 3 & 5i). Strikingly, the bulk of Wag31 interactors are membrane proteins, which might be attributed to the formation of Wag31 oligomers on the membrane. Our results identify MurG, SepIVA, which regulates MurG (47), the D-aminopeptidase Msm2092 and AmiB, both of which are PG remodellers, as Wag31 interactors. Together, these results contribute towards our understanding of how Wag31 affects PG synthesis (Fig 3a,d). AccA3 is an interactor of Wag31 (28, 34) and catalyses the first committed step in the synthesis of long-chain fatty acids by forming malonyl-CoA. In addition, Long-chain specific acyl dehydrogenase (LCAD), which we report here to be another interactor of Wag31, catalyses the first step in the β-oxidation of fatty acids, which might explain the accumulation of long chain PEs and long-chain fatty acids.

As mentioned above, the overexpression of Wag31 leads to an upregulation in α-MA levels (Fig. 2h). The localization of the α-MA transporter MmpL3 depends on polar PG levels (57, 58). MurG is an essential enzyme for PG synthesis (59) and we report here that it strongly interacts with Wag31 (Fig. 3a,d). It is tempting to hypothesize that homeostatic control on lipid composition arises from the ability of Wag31 to modulate the activity of enzymes involved in lipid metabolism and PG synthesis. That both depletion and overexpression of Wag31 affects lipid composition is likely also a manifestation of its ability to function as a homotypic tether, where the tethering ability is inherently sensitive to the tether concentration.

Our results are the first to establish a membrane tethering function of Wag31. DivIVA proteins possess an N-terminal membrane-binding domain and a C-terminal coiled-coil domain (50, 60). Our data show that disruption of the N-terminal domain ($Wag31_{\Delta N}$) markedly reduces membrane binding and completely abolishes membrane tethering (Fig. 4f, g). The N-terminal domain binds CL while the C-terminal coiled-coil domain facilitates multimerization, which together could explain the molecular

basis for Wag31 to function in homotypic tethering of CL-containing membranes. Results from testing mutants defective in membrane tethering indicate that this function is important for the proper localisation of CL and eventually the survival of mycobacteria (Fig. 5f & 6c-d). Thus, alterations in the native levels of Wag31 results in a displacement of CL from the poles (Fig. 5a-d). However, given NAO's ability to bind to anionic phospholipids (albeit with lower affinity), a smaller degree of NAO redistribution intensity might be coming indirectly from other anionic phospholipids displaced from the membrane due to the loss of membrane integrity or cell shape changes caused by Wag31 depletion.

While, complementation with Wag31 reverses the phenotypic changes observed upon Wag31 depletion, complementation with the membrane tethering-defective mutant ($Wag31_{\Delta N}$) fails to do so (Fig. 5f-g & 6a-d). These results not only highlight the dependence of CL localization on membrane-tethering but also underscores the importance of tethering for maintaining cellular morphology, physiology and survival. CL micro-domains at the poles (52, 53) have been shown to be an important hub for protein localisation and activity. Several studies have implicated CL in modulating the activities of membrane-resident proteins involved in electron-transport, protein translocation, bacterial two-component system etc. (61-64). Our work delineates the roles of the N- and C-terminal domains of Wag31. The N-terminal DivIVA-domain facilitates lipid binding and membrane tethering, and the C-terminal coiled-coil domain engages in protein-protein interactions and facilitates the multimerization of Wag31. This is evident from findings that deletion of the N-terminal DivIVA-domain affects lipid binding and tethering but not its ability to bind interacting partners (Fig. 4c-d, f-g & 7c). Based on our results, we propose a model in which the N-terminal of Wag31 binds and tethers CL ensuring its proper localization while the C-terminal is free to interact and recruit proteins to the membrane to facilitate cell growth and division (Fig. 8). We reason that the loss of cell-shape and viability in the absence of tethering occurs due to mis-localization of CL which in turn has a negative impact on membrane-localized processes at a global scale.

Materials and Methods

All the illustrations were made using BioRender. List of constructs and strains used in the study are given in Table S1. Mass spectrometry samples were processed and performed by Valerian Chem.

Bacterial strains and culturing

Middlebrook 7H9 medium (BD Biosciences) or 7H11 agar (BD Biosciences) was used to cultivate mycobacterial strains. 7H9 medium was supplemented with 10% ADC (albumin, dextrose, NaCl, and catalase) and 0.2% glycerol (Sigma) and, 0.05% Tween-80 (Sigma) or 7H11 agar (BD Biosciences) with 10% OADC (oleic acid added to ADC) and 0.2% glycerol were added to the media. Antibiotic concentrations used: Hygromycin (Hyg) was used at 100 µg/mL, Kanamycin (Kan) at 25 µg/mL, and Apramycin (Apra) at 30 µg/mL for *Msm*. *E. coli* was cultured in Miller Luria Bertani Broth (Himedia) or Miller Luria Bertani Agar. Antibiotic concentrations used: Hyg was used at 150 µg/mL, Kan at 50 µg/mL, Apra at 30 µg/mL, Ampicillin (Amp) at 100 µg/mL for *E. coli*.

Generation of *wag31* conditional mutant and *in vitro* Growth kinetics

Recombineering method, as described in (65), was used to generate a Wag31 conditional gene replacement mutant. First, wag31 was cloned under a tet regulatable promoter in pST-KiT$_{off}$ (kan res; (66)), which turns off transcription upon the addition of anhydrotetracycline. pST-wag31 construct thus generated was electroporated into a recombineering proficient strain, Msm::pJV53. An allelic exchange substrate was generated by cloning 675 bp from upstream (Left hand sequence, LHS) and 700 bp from downstream (Right hand sequence, RHS) of *wag31* (including ~150 bp at both ends) with *hyg*^{res} cassette and *oriE+cosλ* and digested with SnaBI to release the donor LHS-hyg^{res}-RHS. The linear donor was electroporated into Msm::wag31 expressing gp60 and gp61 recombinases. The colonies were selected on Hyg and ten colonies were screened with multiple primer pairs to confirm recombination at the native locus. Confirmed recombinants were passaged multiple times to cure them of pJV53 to generate conditional mutant Δwag31.To perform *in vitro* growth kinetics, secondary cultures of *Msm* and *Δwag31* were seeded at a density of A_{600}~ 0.05 and either left untreated or treated with 100 ng/mL ATc for 12 h. At 0 and 12 h, appropriate serial dilutions were plated on 7H11 agar plate and incubated at 37˚C for 2-3 days, and CFUs were enumerated. CFUs were plotted using GraphPad Prism 9 and analysed by performing Two-way ANOVA (0.0021 (**), 0.0002 (***).

Western blot analysis

Msm, Msm::wag31 and *Δwag31* transformants grown in the presence or absence of IVN/ ATc for 12 h and harvested by centrifugation at 4000 rpm for 10 min at 4ºC. The pellets were resuspended in 1:3 (pellet weight: buffer volume) Phosphate Buffer Saline containing 5% glycerol and 1 mM protease inhibitor- PMSF. The resuspension was transferred into pre-equilibrated bead-beating tubes filled to one-fourth with 0.1mm Zirconia beads. Pre-equilibration was performed by washing the beads with autoclaved MilliQ followed by lysis buffer. The tubes were placed in a bead-beater and subjected to 6-8 cycles of bead-beating -1 min on and 2 min rest on ice. To obtain WCL, the tubes were centrifuged at 13000 rpm for 10 min at 4˚C, and the supernatant was collected in a microcentrifuge tube. The concentration of protein in each sample was estimated by Pierce BCA protein Assay kit (Thermo Fischer Scientific), and 40 µg WCLs were resolved on 10-12% SDS-PAGE gels at constant current and transferred onto Nitrocellulose (NC) membrane. This was followed by blocking the membrane with 5%

Bovine Serum Albumin (BSA) for an hour at RT and subsequently incubating it with the desired primary antibody for 2 h at RT or overnight at 4˚C. The primary antibodies used were either anti-RpoA (raised in rabbit), anti-Wag31 (raised in rabbit), anti-FLAG (raised in mice, Sigma), anti-His (raised in rabbit, CST). The membrane was washed thrice for 10 min each with PBST (PBS + 0.5% Tween-20) to remove any non-specific binding. Next, the membrane was probed with appropriate secondary antibody (anti-rabbit, Invitrogen or anti-mice, Invitrogen) for an hour at RT, washed thrice for 10 min each with PBST, developed using ECL reagent (Millipore) and visualized on BioRad ChemiDoc Touch Gel imaging system.

Sample preparation for SEM and TEM

Msm and *Δwag31* were set up at A_{600}~0.05 and grown overnight in either the presence of absence of 100 ng/ml ATc. Post 12 h, the cells were harvested by centrifugation at 4000 rpm for 10 min at RT. Cells equivalent to A_{600} ~2 were taken further for sample preparation and washed thrice with 5 mL sterilized PBS. The cells were fixed with 5 mL of fixative (4% Paraformaldehyde (Sigma), 2.5% Glutaraldehyde (EMS), 0.1M Na-Cacodylate) for 4 h at RT protected from light. Cells were tap-mixed every 30 min to ensure that they remained in suspension. This was followed by washing the cells twice for 10 min with 0.1 M Na-Cacodylate buffer. Subsequently, cells were stained with 3 mL of 1% Osmium Tetraoxide (Os_4O_2) protected from light for a maximum of 1.5 h with tap-mixing every 30 min. Os_4O_2 was removed from the samples by centrifugation at 4000 rpm at 10 min at RT and discarded as per safety guidelines. The cells were then subjected to serial dehydration at RT with increasing concentrations of ethanol from 25% to 100%. Briefly, the cells were incubated for 5 min with 25% ethanol, harvested, and incubated for 7 min with 50% ethanol. This was followed by serially incubating the cells for 15, 20, and 30 min for 75%, 95%, and 100% (thrice) ethanol, respectively. Cells were then taken forward for critical-point drying with the help of 100 µl Hexamethyldisilazine (HMDS). Meanwhile, stubs were prepared by placing carbon tape and coverslip on them. 10 µl of the dried sample was spotted on the coverslip and evenly spread. Next, the stub was coated with 0.8 mm Gold and stored in a desiccator or imaged at 20,000X using FEI Nova NanoSEM 450. For TEM, cells were grown and harvested as described above for SEM. For TEM sample preparation, 50 OD cells were taken, fixed, stained, and gradually dehydrated with ethanol, as explained above. The cells were then infiltrated with Epon 812 resin. This was followed by cutting the resin into several 62 nm thick ultra-thin sections using an ultramicrotome (Leica EM UC7). The sections were then stained with Uranyl acetate and lead citrate and examined on a 120 kV transmission electron microscope (L120C, Talos, Thermo Scientific) at 17,500 magnification.

BODIPY labelling, imaging and analysis

1 mL cells of *Msm* and *Δwag31* either untreated or treated with 100 ng/mL ATc for 12 h were stained with 20 µg/mL BODIPY (Invitrogen). For examining lipids in Wag31 overexpression strain, *Msm* and *Msm::wag31* were treated with 5 µM IVN for 12 h and 1 mL cells of both strains were stained with 2.5 µg BODIPY. Staining was performed for 30 min protected from light in an incubator shaker followed by washing with sterilized Phosphate buffer saline (PBS). For Msm and Δwag31, ~10 µl of cells were spotted on a 1% agar pad (prepared in 7H9) and visualized using a 100X/1.4 NA oil immersion objective on a Zeiss, LSM880 at 488 nm/510 nm (Excitation: Emission). Background correction in the collected images

followed by Corrected Total Cell Fluorescence analysis was performed using Fiji (2) and plotted using Graph Pad Prism 9. For examining lipids in BODIPY-stained Msm and Msm::wag31, 2 μl of cells were spotted on a 1% agar pad (prepared in 7H9) and visualized using a 100X/1.32 NA oil immersion objective on a Leica THUNDER Imaging systems at 475nm:519nm (Excitation: Emission). About 20 Z-stack images, each spaced 0.1 μM apart, were acquired using a scientific CMOS K8 camera (Leica microsystems). Background correction and Thunder image processing was performed on the images using the Las-X software module (Leica microsystems). Processed images were then analysed for CTCF using Fiji (2) and plotted using Graph Pad prism 9.

Sample preparation for Lipidomics and analysis

Secondary cultures of *Msm* and *Δwag31* were seeded at a density of A600~ 0.05 and either left untreated or treated with 100 ng/mL ATc for 12 h until A600~ 0.8-1.0. Post 12 h incubation with ATc, Cells corresponding to A_{600}~20 were harvested and processed for lipid extraction. Bacterial pellets were resuspended in 1 ml sterilized PBS and transferred to a 3 ml glass vial. 2:1 Chloroform::Methanol mixture was added to it and vortexed vigorously for 2 min. Chloroform contained 1 nm 15:0 FFA to be used as the internal standard for normalization. The samples were centrifuged at 1500 rpm for 5 min at RT to separate the organic layer. The latter was transferred to a new glass vial, and 2 ml Chloroform (containing 2% Formic acid) was added to the old vial to extract phospholipids from the sample. The samples were centrifuged at 1500 rpm for 5 min at RT to extract the phospholipid-containing organic layer. Both organic layers were pooled and dried under a stream of Nitrogen gas at RT. The dried lipid extracts were re-solubilized in 200 µL of 2:1 CHCl3: CH_3OH, and 10 µL was injected into an Agilent 6545 QTOF (quadrupole-time-of-flight) instrument for semi-quantitative analysis using high-resolution auto MS/MS methods and chromatography techniques. A Gemini 5U C-18 column (Phenomenex) coupled with a Gemini guard column (Phenomenex, 4x3 mm, Phenomenex security cartridge) was used for LC separation. The solvents used for negative ion mode were buffer A: 95:5 H2O:CH_3OH + 0.1% ammonium hydroxide and buffer B: 60:35:5 Isopropanol: CH_3OH:H2O + 0.1% ammonium hydroxide. The 0.1% ammonium hydroxide in each buffer was replaced by 0.1% Formic acid + 10 mM Ammonium Formate for positive ion mode runs. All LC/MS runs were for 60 min, starting with 0.3 mL/min 100% buffer A for 5 minutes, 0.5 mL/min linear gradient to 100% buffer B over 40 minutes, 0.5 mL/min 100% buffer B for 10 minutes, and equilibration with 0.5 mL/min 100% buffer A for 5 minutes. The following settings were used for the ESI-MS analysis: drying gas and sheath gas temperature: 320°C, drying gas and sheath gas flow rate: 10 L/min, fragment or voltage: 150 V, capillary voltage: 4000 V, nebulizer (ion source gas) pressure: 45 psi and nozzle voltage: 1000 V. For analysis, a lipid library was employed in the form of a Personal Compound Database Library (PCDL), and the peaks were validated based on relative retention times and fragments obtained. This library was selectively curated from the MycoMass database and the LIPID MAPS Structure Database (LMSD). All robustly detected lipid species were quantified by normalizing areas under the curve (AUC) to the AUC of the relevant internal standard added and by normalizing to the total cell number. Log2 fold changes were then plotted for each lipid compared to the Msm-ATc samples.

Immunoprecipitation (IP) and MS/MS analysis

250 mL secondary cultures of *Msm*::*gfp* and *Δwag31* were inoculated at an A600~ 0.05 and

incubated in a shaker incubator until A_{600}~ 0.8-1.0. Cells were collected and lysed using bead-beating to make Whole cell lysate (WCL) and passed through a 0.2 µM filter. 3 mg lysate from each group was immunoprecipitated overnight with anti-FLAG® M2 magnetic beads (Millipore), washed thrice, and heated in 4X Laemmli Buffer. One-fifth of the IP supernatant was resolved on a 10% gel, transferred onto a Nitrocellulose membrane, and probed with anti-FLAG Antibody (Sigma). Lysates from confirmed IPs (biological quadruplets) were taken further for mass spectrometry sample preparation and analysis. Sample preparation and, mass spectrometry analysis were outsourced to VProteomics, New Delhi. Briefly, the IP samples were reduced with 5 mM TCEP, followed by alkylation with 50 mM iodoacetamide. The samples were digested with 1µg Trypsin for 16 h at 37 °C. Digests were cleaned using a C18 silica cartridge and resuspended in a buffer containing 2% acetonitrile and 0.1% formic acid. 1 µg of peptide was used for analysis in an Easy-nlc-1000 system coupled to an Orbitrap Exploris mass spectrometer. The gradients were run for 110 min. MS1 spectra were acquired in the Orbitrap (Max IT = 60 ms, AGQ target = 300%; RF Lens = 70%; R=60K, mass range = 375−1500; Profile data). Dynamic exclusion was employed for 30 seconds, excluding all charge states for a given precursor. MS2 spectra were collected for the top 20 peptides. MS2 (Max IT=60ms, R= 15K, AGC target 100%). Proteome Discoverer (v2.5) was used to analyse the RAW data against the Uniprot Msm database. The precursor and fragment mass limitations for the dual Sequest and Amanda searches were established at 10 ppm and 0.02 Da, respectively. The false discovery rate for proteins and peptide spectrum matches was adjusted to 0.01 FDR. For identification of interactors unique to Wag31, we removed all the proteins obtained in the three replicates of *Msm::gfp* from the *Δwag31* datasets. In the corrected datasets, proteins common to all the three replicates with minimum unique peptides #2 were considered interactors. To identify top hits, PSM cut-off was set to 18 and unique peptides to 5.

Protein expression and purification

BL21(DE3) cells transformed with pET-wag31, or pET-wag31K20A or pET-wag31$_{\Delta N}$ were cultured at 37ºC until the A600 ~0.6. 0.1 mM IPTG was added to the culture to induce protein expression, followed by incubating the culture at 18ºC for 12 h. Cells were pelleted and stored at -40 ºC. The bacterial pellet was resuspended in a lysis buffer (20 mM HEPES pH 7.4, 150 mM NaCl, and 20 mM imidazole with 1 mM phenylmethylsulphonyl fluoride (PMSF)) and lysed by sonication in an ice-water bath. Lysate was spun at 30,000 x g for 20 min, and the supernatant obtained was incubated with TALON® Metal Affinity Resin (Takara Bio) 4 ºC for 30 min. The resin was extensively washed with lysis buffer, and the bound protein was eluted with 20 mM HEPES pH 7.4, 150 mM NaCl, and 250 mM imidazole. The elution was dialyzed against 20 mM HEPES pH 7.4 150 mM NaCl and stored at 4 ºC for the duration of the experiments. Aggregates were removed by centrifugation at 100,000 g. Concentration of the proteins was quantified by measuring A280 using the molar extinction coefficient predicted by the Expasy ProtParam tool.

Liposome preparation

1,2-dioleoyl-sn-glycero-3-phosphocholine (DOPC), 1,2-dioleoyl-sn-glycero-3-phosphoethanolamine (DOPE) and1′,3′-bis[1,2-dioleoyl-sn-glycero-3-phospho]-glycerol (sodium salt), CL were obtained from Avanti Polar Lipids. 1,1'-dilinoleyl-3,3,3',3'-tetramethylindocarbocyanine, 4-chlorobenzenesulfonate (FAST DiI™), and 3,3'-dilinoleyloxacarbocyanine perchlorate (FAST DiO™)

were obtained from Invitrogen. The UV-activable, diazirine-containing reactive fluorescent lipid probe BODIPY-diazirine phosphatidylethanolamine (BDPE) was prepared as described earlier (1, 2). For liposome preparation, lipids were aliquoted from chloroform stocks at desired ratios in a clean glass tube and dried under a high vacuum for an hour to a thin film. The dried lipids were used at a final concentration of 1 mM (deionised water was added to them). After hydrating at 50 °C for 30 minutes, lipids were vigorously vortexed and then extruded through polycarbonate filters with pore sizes of 100 nm (Whatman). For PLiMAP assays, liposomes were CL, DOPG, or DOPE with 69 mol% DOPC and 1 mol% BDPE. Liposomes used in tethering assays were made similarly with 30 mol% CL or DOPE and 1 mol% of the fluorescent lipid DiI or DiO) in the DOPC background.

Proximity-Based Labelling of Membrane-Associated Proteins (PLiMAP)

For carrying out the PLiMAP assay, Wag31 and its mutants were purified and desired liposomes were prepared as described in supplementary. PLiMAP was carried out and analysed as described (67). Briefly, 2 µM Wag31 or its mutants were incubated with liposomes containing 30 mol% CL, DOPG, or DOPE (200 µM total lipid) in a final volume of 30 µL. The reaction was incubated for 30 min in the dark at room temperature followed by exposure to a 1 min long pulse of 365 nm UV light (UVP crosslinker CL-1000L) at an intensity of 200mJ cm^{-2}. The reaction was mixed with Laemmli sample buffer, boiled, and equal volumes for all reactions were loaded onto a 10% polyacrylamide gel and resolved using SDS-PAGE. iBright1500 (Thermo Fischer Scientific) or Amersham Typhoon (GE) were used for imaging gels. Gels were first imaged for BODIPY fluorescence and later fixed and stained with Coomassie Brilliant Blue.

Tethering assays, fluorescence imaging, and image analysis

1 µM of Wag31 and its mutants were mixed with 10 µM of 100 nm extruded liposomes in Eppendorf. The mixture was then transferred to a LabTek chamber and imaged using 100x 1.4 NA oil-immersion objective on an Olympus IX73 inverted microscope connected to an LED light source (CoolLED) and an Evolve 512 EMCCD camera (Photometrics). Image acquisition was controlled by µManager, and images were analysed using Fiji. For single liposome intensity analysis, all images from the same condition from two independent experiments were combined into one montage. The montage was duplicated and thresholded using Fiji's Otsu algorithm to generate a binary mask. The mask was overlaid onto the original montage to obtain the maximum intensity of liposomes.

NAO labelling, imaging and analysis

Msm, *Msm::wag31* were treated with 5 µM IVN for 12 h and *Msm* and *Δwag31* were either left untreated or treated with 100 ng/mL ATc for 12 h. For complementation experiment, 1 mL of each strain was stained with 2 µM NAO for 1 h protected from light in an incubator shaker and washed thrice with sterilised 1X PBS. 2 µl of cells were spotted on a 1% agar pad (prepared in 7H9) and visualized using a 100X/1.32 NA oil immersion objective on a Leica THUNDER Imaging systems at 475nm:535nm (Excitation: Emission). About 20 Z-stack images, each spaced 0.1 µM apart, were acquired using a scientific CMOS K8 camera (Leica microsystems). For CL specific labelling, collection was also performed at 642nm.

Background correction and Thunder image processing was performed on the images using the Las-X software module (Leica microsystems). Processed images were then analysed using Fiji (68)and

plotted using Graph Pad prism 9. Briefly, N=100 cells across two independent experiments were examined for their profile of CL distribution by normalizing the cell length and assigning pole with brighter NAO fluorescence intensity as 0 and the other pole as 100. The fluorescence intensity was normalised to the highest fluorescent value for each cell. Corresponding fluorescence intensity value for all cells for every point between 0 to 100 were calculated from the LOOKUP function of excel. The values representing CL fluorescence across 100 cells were averaged out and plotted against normalised cell length in GraphPad prism 9. 0th order smoothening with 4 neighbours on each size was performed on the curves obtained.

Complementation experiment

Secondary cultures of *Msm, Δwag31, Δwag31::wag31, Δwag31::wag31*$_{K20A}$, and *Δwag31::wag31*$_{\Delta N}$ were set up at A_{600} ~0.05. For each strain, two types of cultures were set up in triplicates- untreated and treated with 100ng/mL ATc and grown for 12 h. At 0 and 12 h, appropriate serial dilutions were plated on 7H11 agar plates and incubated at 37˚C for 2-3 days. CFUs were enumerated and plotted using GraphPad Prism 9. Statistical analysis was performed using two-way RM ANOVA followed by *Tukey's* multiple comparison test, α=0.01, GP: 0.1234 (ns), 0.0332 (*), 0.0021 (**), 0.0002 (***), <0.0001 (****). For BODIPY- and NAO- labelling, the strains were grown as described above. At 12 h, 1 mL cultures of *Msm*+ATc, *Δwag31, Δwag31* +ATc, *Δwag31::wag31*+ATc, *Δwag31::wag31*$_{K20A}$ +ATc, and *Δwag31::wag31*$_{\Delta N}$ +ATc were taken and labelled with either BODIPY or NAO. The labelling, imaging and analysis for both fluorophores was performed as described in the respective sections above.

His pulldown assay.

BL21 (DE3) cells transformed with no plasmid, or pET-wag31 or pET-wag31$_{\Delta N}$ or pET-wag31$_{\Delta C}$ were cultured and cell lysates were prepared as described for PLiMAP and tethering assays. Wag31 or Wag31$_{\Delta N}$ was assessed by resolving the samples on 10% SDS-PAGE followed by Coomassie staining whereas Wag31$_{\Delta C}$ was resolved on Tris-Tricine PAGE as described elsewhere (69). The interacting partners, namely *murG*, *sepIVA*, *msm2092* and *accA3* and the non-interactor *mmpS5* were amplified from Msm genomic DNA using gene specific primers harbouring NdeI-HindIII sites and amplicons were digested and cloned into the corresponding sites in pNit-3X-FLAG shuttle vector. The constructs thus generated were electroporated in *Msm* to generate *Msm::murG*, *Msm::SepIVA*, *Msm::msm2092*, *Msm::accA3* and *Msm::mmpS5*. The cultures grown till A600 ~0.8 were used for fresh inoculation at A_{600} of 0.05 in 7H9 media containing 0.5 μM IVN. Cultures were grown for 12 h and lysates were prepared by bead-beating and 40 μg were resolved on 10% gels and probed with α-FLAG antibody.

500 μg of *E. coli* lysates expressing Wag31 or mutant were mixed with 300 μg *Msm* lysates expressing Wag31 interactors in a total reaction volume of 700 μL and the samples were twirled at 4ºC for 2 h. 50 μL cobalt beads/ sample (GoldBio) were washed twice with lysis buffer and incubated with 5% BSA solution for 2 h at 4ºC. Subsequently, beads were washed with lysis buffer and incubated with samples for 2 h (twirled at 4ºC). The pull downs were washed thrice in lysis buffer containing 1%

Triton X-100 and finally resuspended in 2X-SDS sample buffer. Pulldown samples were resolved on 10-12% SDS-PAGE and probed with α-His and α-FLAG antibodies.

Figure Legends:

Fig.1| Loss of Wag31 leads to the formation of Intracellular Lipid Inclusions (ILIs).

(a.) Illustration depicting the known role of Wag31 in directing polar elongation and maintaining rod-shaped morphology of cells. **(b.)** Whole Cell Lysates **(**WCL) were prepared from *Msm* and *Δwag31* (Table S1) either untreated or treated with 100 ng/mL ATc for 12 h, and 40 µg lysate was resolved on a 12% gel, transferred on Nitrocellulose membrane, and probed with either α-Wag31 or α-rpoA antibody (loading control), respectively. **(c.)** Cultures showing growth of *Msm* and *Δwag31* either untreated or treated with 100 ng/mL ATc for 12 h. **(d.)** *Msm*+ATc, *Δwag31*-ATc, and *Δwag31*+ATc were tracked for bacillary survival at 0 and 12 h by enumerating CFUs. Appropriate serial dilutions were plated on 7H11 plates (without antibiotic or ATc), and bar graphs demonstrating bacillary survival (CFU $\log_{10}$/mL ± standard deviations (SD, represented by error bars) were plotted at indicated time points. Statistical significance was calculated using Two-way ANOVA (0.0021 (**), 0.0002 (***). The experiment was performed twice independently, each performed in triplicates. **(e.)** SEM micrographs showing *Msm*, *Δwag31*-ATc, and *Δwag31*+ATc at 12 h post-treatment. **(f.)** Cells depicting rod, bulged or round morphology. The yellow arrowhead indicates bulged pole of the cell. **(g.)** 200 cells from each group were checked for either rod, bulged or round morphology, and the percentage of cells with these morphologies in all the three strains was plotted in a bar graph. **(h.)** TEM micrographs showing *Msm*, *Δwag31*-ATc, and *Δwag31*+ATc at 12 h post-treatment. **(i.)** 250 cells, each from *Msm*, *Δwag31*-ATc and 185 cells from *Δwag31*+ATc, were divided into three classes (0-2, 2-5, and >5 ILIs) based on the number of ILIs and the percentage of each class in every strain was plotted in a bar graph.

Fig.2| Wag31 levels perturb lipid homeostasis

Representative micrographs showing BODIPY staining in **(a.)** *Msm*+ATc, *Δwag31*-ATc and, *Δwag31*+ATc samples imaged 12 h post-ATc treatment **(b.)** *Msm*+ IVN, *Msm*::*wag31* + IVN samples imaged 12 h post 5 µM IVN treatment. **(c.)** Corrected total cell fluorescence was calculated in individual bacterial cells from *Msm*+ATc, *Δwag31*-ATc, and *Δwag31*+ATc strains (N=48) and plotted in a graph. Horizontal bar represents median CTCF. (Statistical analysis was performed using one-way ANOVA followed by Brown-Forsythe test (Tukey's multiple comparison test; 0.0021 (**), <0.0001 (****)). **(d.)** Corrected total cell fluorescence was calculated for 42 individual cells from *Msm*+IVN, and *Msm*::*wag31*+IVN strains and plotted in a graph (Statistical analysis was performed using Welch's t-test 0.0021 (**), **e.)** Schematic depicting the workflow of Lipidomics (LC-MS). **(f-g.)** Heatmap depicting $\log_2$ fold change (FC) in indicated lipid classes of *Msm* +ATc, *Δwag31*-ATc, and *Δwag31+ATc* as compared to *Msm*-ATc. The experiment was performed with six biological replicates, and the abundances of identified lipid classes were normalized to *Msm*-ATc to yield relative abundances of lipids in other strains. Blue and red colours indicate upregulated and downregulated lipid classes; color intensity variation changes with $\log_2$ FC. **(h.)** Bar graph (Mean ± SEM) depicting the abundance of α-MA in *Msm* and *Msm::wag31* treated with 5 µM IVN for 12 h. Values on the Y-axis represent area under the curve (AUC) normalised to an internal standard (FFA 15:0). X-axis represent various species (chain length variations) of α-MA. (Statistical analysis was performed using two-way ANOVA followed by a Tukey's multiple comparison's test; <0.0001 (****)).

Fig.3| Molecular interactions of Wag31 with membrane-associated proteins govern cellular homeostasis.

(a.) Illustration showing the distribution of the top 20 interactors of Wag31 identified from MS/MS analysis from three independent immunoprecipitations. Interactors were classified on the basis of their functional category based on data available in Mycobrowser (70). MSMEG numbers or the identity of interactors are marked in smaller circles. **(b.)** Coomassie Brilliant blue (CBB) staining of plain *E.coli* lysate and *E.coli* lysate expressing His-Wag31*. E. coli* lysate prepared from BL21-DE3 strain was used as the control. **(c.)** Representative western blots demonstrating expression of 3XFLAG tagged-MurG, -SepIVA and -Msm2092. WCLs were prepared from 0.5 μM IVN induced *Msm::murG*, *Msm::sepIVA, Msm::msm2092* and 40 μg of each was resolved on a 10 % SDS-PAGE, transferred onto a nitrocellulose membrane and probed with α-FLAG and α-RpoA (loading control). **(d.)** Representative western blots showing interaction of MurG, SepIVA, and, Msm2092 with Wag31. *Msm* and *E. coli* lysates represented in (b & c) incubated together and pulled down with Cobalt beads were resolved on a 10-12 % SDS-PAGE, transferred onto nitrocellulose membrane and probed with α-His to detect the pulldown and α-FLAG to detect the interaction. The experiment was performed independently twice.

(e.) Graphic representation (adapted from (48)) shows the distribution of the top 20 interactors in different compartments of a mycobacterial cell: membrane, cytoplasm, or core (involved in DNA replication and recombination). Interactors from each compartment are marked inside the respective domain. **(f.)** Pie-chart shows the distribution of interactors belonging to the IMD, PM-CW, or membrane proteins whose specific localization is not determined. Percentage of proteins (top 20 hits) belonging to each membrane-compartment is mentioned.

Fig.4| Wag31 binds and tethers mycobacterial membrane.

(a.) Schematic showing the workflow of the PLiMAP assay. **(b.)** Coomassie Brilliant blue (CBB) staining of His-Wag31 and in-gel fluorescence (FI) from a representative PLiMAP experiment performed using 2 μM Wag31 and hundred-fold excess of 30 mol% of either 1,2-dioleoyl-sn-glycero-3-phosphoethanolamine (DOPE-), and1′,3′-bis[1,2-dioleoyl-sn-glycero-3-phospho]-glycerol (DOPG-), or CL-containing liposomes. **(c.)** CBB and FL gels from a representative PLiMAP experiment performed with 2 μM Wag31, $Wag31_{K20A,}$ or $Wag31_{\Delta N}$ either in the presence or absence of 30 mol% CL liposomes. Note the presence of SDS-resistant higher-order polymers in gel indicated by the red curly bracket. **(d.)** Quantitation of PLiMAP data from (c.) showing a difference in binding propensities of His-Wag31, His-$Wag31_{K20A}$ and His-$Wag31_{\Delta N}$. Data represent the mean ± SD of three independent experiments. Statistical analysis was performed using a 2-tailed unpaired student's t test in Graph Pad Prism 9. Wag31 vs $Wag31_{K20A}$ showed no significant difference (ns, p value = 0.5667) whereas Wag31 vs $Wag31_{\Delta N}$ (p value = 0.0081, **) and $Wag31_{K20A}$ vs $Wag31_{\Delta N}$ (p value = 0.0002, ***) showed significant difference in binding **(e.)** Representative micrographs from binding and tethering assay showing CL-Dil-liposomes (~100 nm) before (first panel) and after incubation (second panel) with 1 μM His-Wag31-GFP. Membrane and protein fluorescence are rendered in red and green, respectively. The experiment was performed independently twice. **(f.)** Representative micrographs from tethering experiments performed with His-Wag31, His-$Wag31_{K20A,}$ or His-$Wag31_{\Delta N}$ proteins. The left panels indicate PE

liposomes only (upper panel) and PE liposomes incubated with 1 μM Wag31 (lower panel), the middle panels indicate CL liposomes (upper) or CL liposomes incubated with 1 μM Wag31 (lower panel), the right panel indicates CL liposomes either incubated with His-Wag31$_{K20A}$ (upper) and His-Wag31$_{\Delta N}$ (lower). For visualization, PE- and CL-containing liposomes were doped with trace amounts of 3,3'-dilinoleyloxacarbocyanine perchlorate (FAST DiO™) and 4-chlorobenzenesulfonate (FAST DiI™), respectively**. (g.)** Data from particle analysis showing the maximum intensity of liposomes for all the reactions from two independent experiments.

Fig.5| Tethering is crucial for the survival of mycobacteria

(a.) Top panel: Representative Fluorescent micrographs showing NAO intensity across *Msm*+ATc, *Δwag31*-ATc and, *Δwag31*+ATc samples imaged at 12 h post-ATc treatment. Bright red foci of polar CL are indicated with yellow arrowheads and septal CL foci with white arrowheads. Bottom panel: shows respective phase images. **(b.)** Line plot depicting CL distribution along the length of the cells across *Msm*+ATc, *Δwag31*-ATc and, *Δwag31*+ATc. N=100 cells across two independent biological replicates were analysed using Fiji and their normalised fluorescence intensities were plotted against cell length; fluorescence emitted from 0-20 % & 80-100 % of cell length was considered polar. **(c.)** Representative fluorescent micrographs showing NAO staining in *Msm*+IVN, *Msm*::*wag31*+IVN samples imaged at 12 h post 5 μM IVN treatment. Bright red foci of polar CL are indicated with yellow arrowheads, and septal CL foci with white arrowheads. The panels below show corresponding phase images. **(d.)** Line plot depicting CL distribution along the length of the cells in *Msm*+IVN, *Msm*::*wag31*+IVN. N=100 cells across two independent biological replicates were analysed using Fiji. The y-axis represents the normalized fluorescence intensities, and the x-axis represents cell length expressed as a percentage of total cell length. Fluorescence peaks in 0-20 % & 80-100 % of cell length were considered polar. **(e.)** Structure of Wag31 (MSMEG_4217) from AlphaFold protein structure database (71). The structure represents the N-terminal, linker, and C-terminal domains in Wag31. The N-terminal contains a short helix, followed by an intertwined loop harbouring positively charged amino acid K20 (highlighted in red) and the DivIVA domain. The N-terminus is linked to the C-terminus via a linker. **(f.)** *Msm*+ATc*, Δwag31, Δwag31::wag31, Δwag31::wag31$_{K20A}$, Δwag31::wag31$_{\Delta N}$* either untreated or treated with ATc were scored for bacillary survival post 12 h ATc addition by enumerating CFUs. Appropriate serial dilutions were plated on 7H11 plates (without antibiotic or ATc), and bar graphs demonstrating bacillary survival (CFU $\log_{10}$/mL ± standard deviations (SD, represented by error bars) were plotted and statistical significance was calculated using two-way RM ANOVA followed by *Tukey's* multiple comparison test, α=0.01, GP: 0.1234 (ns), 0.0332 (*), 0.0021 (**), 0.0002 (***), <0.0001 (****). The experiment was performed twice independently, each with triplicates. **(g.)** Strains described in **(f.)** were scored for their morphology-rod, bulged or round at 12 h post ATc treatment. 308 cells of each strain across two independent experiments were analysed.

Fig.6| Tethering is correlated with lipid levels and CL localization in mycobacteria

(a.) Top panel: Representative fluorescent micrographs showing BODIPY staining across *Δwag31-ATc and Msm, Δwag31, Δwag31::wag31, Δwag31::wag31$_{K20A}$, Δwag31::wag31$_{\Delta N}$* imaged at 12 h post ATc

addition. Bottom panel: corresponding phase images. **(b.)** Corrected total cell fluorescence (CTCF) of BODIPY-stained cells was calculated from N=100 cells across two independent experiments and analysed using Fiji and plotted in a graph. The horizontal bar represents the median CTCF. (Statistical analysis was performed using one-way ANOVA followed by Brown-Forsythe test (Tukey's multiple comparison test; 0.1234 (ns), 0.0332 (*), <0.0001 (****)). **(c.)** Fluorescent micrographs showing NAO intensity of strains as mentioned above. Bottom panel: corresponding phase images. **(d.)** Line plot analysis of strains described in **(c.)** depicting CL localisation. N=100 cells across two independent experiments were analysed using Fiji and their normalised fluorescence intensities were plotted against cell length.

Fig.7| The N and C-terminal domains of Wag31 have distinct functions.

a.) Illustration depicting the domain architecture of Wag31, Wag31$_{\Delta N}$ and Wag31$_{\Delta C}$. **(b.)** Coomassie Brilliant blue (CBB) staining of plain *E. coli* lysate and *E. coli* lysate expressing His-Wag31$_{\Delta C}$. *E. coli* lysate prepared from BL21-DE3 strain was used as the control. **(c.)** Representative western blots demonstrating expression of 3XFLAG tagged-MmpS5, -MurG, -SepIVA, -Msm2092 and, -AccA3. WCLs were prepared from 0.5 µM IVN induced *Msm::mmpS5*, *Msm::murG*, *Msm::sepIVA, Msm::msm2092, Msm::accA3* and 40 µg of each was resolved a 10 % SDS-PAGE, transferred onto a nitrocellulose membrane and probed with α-FLAG and α-RpoA (loading control). **(d.)** Representative western blots showing interaction of MurG, SepIVA, Msm2092 and, Acca3 with Wag31 and Wag31$_{\Delta c}$. The non-interactor MmpS5 was used as a negative control. *E. coli* and *Msm* lysates represented in (b & c) incubated together and pulled down with Cobalt beads were resolved on Tris Tricine gel as described elsewhere (69), transferred onto nitrocellulose membrane and probed with α-His to detect the pulldown and α-FLAG to detect the interaction. The experiment was performed independently twice. **(e.)** Coomassie Brilliant blue (CBB) staining of *E. coli* lysates expressing His-Wag31$_{\Delta N}$. *E. coli* lysate prepared from BL21-DE3 strain was used as the control. **(f.)** Representative western blots demonstrating expression of 3XFLAG tagged-MurG, -SepIVA, -Msm2092 and, -AccA3. WCLs were prepared from 0.5 µM IVN induced *Msm::murG*, *Msm::sepIVA, Msm::msm2092, Msm::accA3* and 40 µg of each was resolved a 10 % SDS-PAGE, transferred onto a nitrocellulose membrane and probed with α-FLAG and α-RpoA (loading control). (g.) Representative western blots showing interaction of MurG, SepIVA, Msm2092 and, Acca3 with Wag31 and Wag31$_{\Delta N}$. *E. coli* and *Msm* lysates represented in (e & f) incubated together and pulled down with Cobalt beads were resolved on 10% SDS-PAGE, transferred onto nitrocellulose membrane and probed with α-His to detect the pulldown and α-FLAG to detect the interaction. The experiment was performed independently twice.

Fig.8| Model for Wag31 mediated tethering of the membrane

a.) Model of Wag31 showing the N- and C-terminals. N-terminal houses the DivIVA-domain that is involved in membrane-tethering and the C-terminal is the protein-binding domain that facilitates interactions of Wag31 with other proteins. **(b.)** Left: Illustration showing Wag31 scaffolds bound to cardiolipin in the membrane via N-terminal, tethering it and creating CL-microdomains at the poles. The C-terminal of Wag31 bound to protein-partners, localize them to the membrane, facilitating several

membrane-centric processes such as PG and lipid synthesis, that ensure mycobacterial survival. The right panel shows the time-dependent consequences of Wag31 depletion i.e. early and late stage. The cells are bulged at one pole and start accumulating ILIs in the early stage and as the time progresses, the effect of Wag31 depletion becomes severe, rendering the cells round and full of ILIs. In the absence of Wag31, CL-microdomains become delocalised due to the loss of tethering, pulling away several membrane-associated proteins causing non-polar growth and loss of curvature.

Figure S1| Generation of Wag31 knockdown

(a.) Schematic showing the *wag31* locus in *Msm* and *Δwag31* and illustrating the strategy utilized to replace *wag31* locus with hygromycin resistance cassette. Primers used for knockout confirmation are indicated as F1, R1, F2, R2, F3 and R3. **(b.)** 1% agarose gels showing confirmatory PCRs performed with different primer sets. The first PCR, or the control PCR, was done using SepIVA (738 bp) primers showing amplicon at ~750bp. It indicates an equal amount of gDNA isolated from *Msm* and *Δwag31* and subsequently used for all PCRs. The next panel shows amplicons from the PCR performed with the F1-R1 pair, which bind to *wag31* locus (~819 bp). They yield an 819 bp amplicon in the case of *Msm* and 819 bp and an additional ~1.5 kb amplicon in the case of *Δwag31.* The third and fourth panels show amplicons amplified using the F2-R2 set (expected amplicon ~1.2 Kb) and F3-R3 set (expected amplicon ~0.9 Kb), which are expected only in the case of *Δwag31* confirming legitimate recombination at the native locus.

Fig.S2| Wag31 levels perturb lipid homeostasis

(a.) Whole Cell Lysates **(**WCL) were prepared from *Msm* and *Msm::wag31* (Table S1) treated with 5 μM IVN for 12 h, and 40 μg lysate was resolved on a 12% gel, transferred on Nitrocellulose membrane, and probed with either α-FLAG or α-rpoA antibody (loading control), respectively. **(b-g)** Bar graphs (Mean ± SEM) depicting the abundance of various lipids classes **(b.)** TAG, **(c.)** DAG, **(d.)** FFA, **(e.)** PE, **(f.)** PI, **(g.)** CL in *Msm* and *Msm::wag31* treated with 5 μM IVN for 12 h. Values on the Y-axis represent area under the curve (AUC) normalised to an internal standard. X-axis represent various species (chain length variations) of the above mentioned lipid classes. The experiment was performed with six biological replicates, and the abundances of identified lipid classes were normalized to *Msm*-IVN to yield relative abundances of lipids in *Msm::wag31* +IVN.

Figure S3| *Molecular interactions of wag31 with membrane proteins govern cellular homeostasis.*

(a.) Western blots showing FLAG-GFP (left panel) and FLAG-Wag31 (right panel) immunoprecipitations. 3 mg lysate from each group was processed for overnight FLAG immunoprecipitations, resolved on a 10% gel, and probed with α-Flag antibody. HC and LC are short for Heavy chain and light chain, respectively. **(b.)** Western blot showing expression of His-Wag31 used for the His pulldown experiments. **(c.)** Representative western blots demonstrating expression of 3XFLAG tagged-MmpL4, -MmpS5 and -Msm2092. WCLs were prepared from 0.5 μM IVN induced *Msm::mmpL4*, *Msm::mmpS5, Msm::msm2092,* and 40 μg of each was resolved on a 10 % SDS-PAGE,

transferred onto a nitrocellulose membrane and probed with α-FLAG and α-RpoA (loading control). **(d.)** Representative western blots showing the absence of interaction of Wag31 with both MmpL4 and MmpS5. Msm2092, a Wag31 interactor was used as a positive control. *E. coli* and *Msm* lysates represented in (b & c) incubated together and pulled down with Cobalt beads were resolved on a 10-12 % SDS-PAGE, transferred onto nitrocellulose membrane and probed with α-His to detect the pulldown and α-FLAG to detect the interaction. The experiment was performed independently twice. **(e.)** Classification of cellular processes that occur in different cellular compartments of *Msm,* as shown in (48).

Figure S4| *Molecular interactions wag31 with membrane proteins govern cellular homeostasis.* The list of Wag31 interactors is classified according to functional categories based on the data available in Mycobrowser. The colour of the textbox indicates localization of the proteins: Pink- membrane, blue-cytoplasm, and core- green.

Table S1

Plasmids and strains used in the study.

Table S2. It depicts unique interacting partners found for Wag31.

Acknowledgments

We thank Dharani Kumar, SEST, University of Hyderabad for helping with imaging of SEM stubs; CCMB for access to its Genomics, Advanced Microscopy, and Electron Microscopy facilities; VIDO, USask for providing infrastructure to carry out some part of the work; Asis Kumar Khuntia for the generation of pET28b-*wag31*$_{K20A}$ and pET28b-*wag31*$_{N}$. YK was supported by a Research Associateship from NIH (Grant 6044-SC23-26). YK and ND acknowledge MITACS for the Globalink Research Award (FR118569) which supported the work carried out at VIDO. ND also acknowledges support from Canadian Institutes of Health Research (CIHR, funding reference number 185715). VIDO receives operational funding from the Government of Saskatchewan through Innovation Saskatchewan and the Ministry of Agriculture and from the Canada Foundation for Innovation through the Major Science Initiatives Fund. DD thanks DBT for Senior Project Associateship (Grant no.: BT/PR13522/COE/34/27/2015). Research in this publication was supported by SERB grant (CRG/2018/001294), Govt. of India, and JC Bose Award (JCB/2019/000015), Govt. of India to VKN. Work in the SSK laboratory was supported by the Swarna Jayanti Fellowship to SSK by SERB, Govt. of India (Grant: SB/SJF/2021-22/01). AC was supported by a Senior research fellowship from CSIR, India. HK thanks the Indian Institute of Science Education and Research, Pune, for a graduate fellowship. TP thanks the Howard Hughes Medical Institute for funding support.

References

1. E. F. Bi, J. Lutkenhaus, FtsZ ring structure associated with division in Escherichia coli. *Nature* **354**, 161-164 (1991).
2. P. A. de Boer, R. E. Crossley, A. R. Hand, L. I. Rothfield, The MinD protein is a membrane ATPase required for the correct placement of the Escherichia coli division site. *Embo j* **10**, 4371-4380 (1991).
3. Z. Hu, A. Mukherjee, S. Pichoff, J. Lutkenhaus, The MinC component of the division site selection system in Escherichia coli interacts with FtsZ to prevent polymerization. *Proc Natl Acad Sci U S A* **96**, 14819-14824 (1999).
4. D. M. Raskin, P. A. de Boer, The MinE ring: an FtsZ-independent cell structure required for selection of the correct division site in E. coli. *Cell* **91**, 685-694 (1997).
5. H. Meinhardt, P. A. de Boer, Pattern formation in Escherichia coli: a model for the pole-to-pole oscillations of Min proteins and the localization of the division site. *Proc Natl Acad Sci U S A* **98**, 14202-14207 (2001).
6. C. L. Woldringh *et al.*, Role of the nucleoid in the toporegulation of division. *Res Microbiol* **141**, 39-49 (1990).
7. M. M. Logsdon, B. B. Aldridge, Stable Regulation of Cell Cycle Events in Mycobacteria: Insights From Inherently Heterogeneous Bacterial Populations. *Front Microbiol* **9**, 514 (2018).
8. J. H. Cha, G. C. Stewart, The divIVA minicell locus of Bacillus subtilis. *J Bacteriol* **179**, 1671-1683 (1997).
9. D. H. Edwards, J. Errington, The Bacillus subtilis DivIVA protein targets to the division septum and controls the site specificity of cell division. *Mol Microbiol* **24**, 905-915 (1997).
10. C. M. Kang, S. Nyayapathy, J. Y. Lee, J. W. Suh, R. N. Husson, Wag31, a homologue of the cell division protein DivIVA, regulates growth, morphology and polar cell wall synthesis in mycobacteria. *Microbiology (Reading)* **154**, 725-735 (2008).
11. C. Jani *et al.*, Regulation of polar peptidoglycan biosynthesis by Wag31 phosphorylation in mycobacteria. *BMC Microbiol* **10**, 327 (2010).
12. M. Letek *et al.*, DivIVA is required for polar growth in the MreB-lacking rod-shaped actinomycete Corynebacterium glutamicum. *J Bacteriol* **190**, 3283-3292 (2008).
13. N. R. Thanky, D. B. Young, B. D. Robertson, Unusual features of the cell cycle in mycobacteria: polar-restricted growth and the snapping-model of cell division. *Tuberculosis (Edinb)* **87**, 231-236 (2007).
14. K. J. Kieser, E. J. Rubin, How sisters grow apart: mycobacterial growth and division. *Nat Rev Microbiol* **12**, 550-562 (2014).
15. L. Nguyen *et al.*, Antigen 84, an effector of pleiomorphism in Mycobacterium smegmatis. *J Bacteriol* **189**, 7896-7910 (2007).
16. L. R. Hammond, M. L. White, P. J. Eswara, ¡vIVA la DivIVA! *J Bacteriol* **201** (2019).
17. H. Stahlberg *et al.*, Oligomeric structure of the Bacillus subtilis cell division protein DivIVA determined by transmission electron microscopy. *Mol Microbiol* **52**, 1281-1290 (2004).
18. K. N. Muchová *et al.*, Oligomerization of the Bacillus subtilis division protein DivIVA. *Microbiology (Reading)* **148**, 807-813 (2002).
19. M. Letek *et al.*, DivIVA uses an N-terminal conserved region and two coiled-coil domains to localize and sustain the polar growth in Corynebacterium glutamicum. *FEMS Microbiol Lett* **297**, 110-116 (2009).
20. M. D. Rigden *et al.*, Identification of the coiled-coil domains of Enterococcus faecalis DivIVA that mediate oligomerization and their importance for biological function. *J Biochem* **144**, 63-76 (2008).
21. K. Choukate *et al.*, Higher order assembling of the mycobacterial polar growth factor DivIVA/Wag31. *J Struct Biol* **209**, 107429 (2020).
22. K. Flärdh, Essential role of DivIVA in polar growth and morphogenesis in Streptomyces coelicolor A3(2). *Mol Microbiol* **49**, 1523-1536 (2003).
23. D. Fadda *et al.*, Streptococcus pneumoniae DivIVA: localization and interactions in a MinCD-free context. *J Bacteriol* **189**, 1288-1298 (2007).
24. K. G. Kaval, S. Halbedel, Architecturally the same, but playing a different game: the diverse species-specific roles of DivIVA proteins. *Virulence* **3**, 406-407 (2012).
25. H. B. Thomaides, M. Freeman, M. El Karoui, J. Errington, Division site selection protein DivIVA of Bacillus subtilis has a second distinct function in chromosome segregation during sporulation. *Genes Dev* **15**, 1662-1673 (2001).
26. K. G. Kaval, S. Hauf, J. Rismondo, B. Hahn, S. Halbedel, Genetic Dissection of DivIVA Functions in Listeria monocytogenes. *J Bacteriol* **199** (2017).

27. K. G. Kaval, J. Rismondo, S. Halbedel, A function of DivIVA in Listeria monocytogenes division site selection. *Mol Microbiol* **94**, 637-654 (2014).

28. X. Meniche *et al.*, Subpolar addition of new cell wall is directed by DivIVA in mycobacteria. *Proc Natl Acad Sci U S A* **111**, E3243-3251 (2014).

29. E. S. Melzer, C. E. Sein, J. J. Chambers, M. S. Siegrist, DivIVA concentrates mycobacterial cell envelope assembly for initiation and stabilization of polar growth. *Cytoskeleton (Hoboken)* **75**, 498-507 (2018).

30. W. X. Xu *et al.*, The Wag31 protein interacts with AccA3 and coordinates cell wall lipid permeability and lipophilic drug resistance in Mycobacterium smegmatis. *Biochem Biophys Res Commun* **448**, 255-260 (2014).

31. M. T. M. Hannebelle *et al.*, A biphasic growth model for cell pole elongation in mycobacteria. *Nat Commun* **11**, 452 (2020).

32. I. Santi, N. Dhar, D. Bousbaine, Y. Wakamoto, J. D. McKinney, Single-cell dynamics of the chromosome replication and cell division cycles in mycobacteria. *Nat Commun* **4**, 2470 (2013).

33. P. Mukherjee *et al.*, Novel role of Wag31 in protection of mycobacteria under oxidative stress. *Mol Microbiol* **73**, 103-119 (2009).

34. N. Habibi Arejan *et al.*, Polar protein Wag31 both activates and inhibits cell wall metabolism at the poles and septum. *Front Microbiol* **13**, 1085918 (2022).

35. Y. S. Morita *et al.*, Compartmentalization of lipid biosynthesis in mycobacteria. *J Biol Chem* **280**, 21645-21652 (2005).

36. J. M. Hayashi *et al.*, Spatially distinct and metabolically active membrane domain in mycobacteria. *Proc Natl Acad Sci U S A* **113**, 5400-5405 (2016).

37. A. García-Heredia *et al.*, Membrane-partitioned cell wall synthesis in mycobacteria. *Elife* **10** (2021).

38. V. Singh *et al.*, Identification of aminopyrimidine-sulfonamides as potent modulators of Wag31-mediated cell elongation in mycobacteria. *Mol Microbiol* **103**, 13-25 (2017).

39. J. Daniel, H. Maamar, C. Deb, T. D. Sirakova, P. E. Kolattukudy, Mycobacterium tuberculosis uses host triacylglycerol to accumulate lipid droplets and acquires a dormancy-like phenotype in lipid-loaded macrophages. *PLoS Pathog* **7**, e1002093 (2011).

40. C. Barisch, P. Paschke, M. Hagedorn, M. Maniak, T. Soldati, Lipid droplet dynamics at early stages of Mycobacterium marinum infection in Dictyostelium. *Cell Microbiol* **17**, 1332-1349 (2015).

41. R. Bartz *et al.*, Lipidomics reveals that adiposomes store ether lipids and mediate phospholipid traffic. *J Lipid Res* **48**, 837-847 (2007).

42. K. Tauchi-Sato, S. Ozeki, T. Houjou, R. Taguchi, T. Fujimoto, The surface of lipid droplets is a phospholipid monolayer with a unique Fatty Acid composition. *J Biol Chem* **277**, 44507-44512 (2002).

43. A. Griego, T. Douché, Q. G. Gianetto, M. Matondo, G. Manina, RNase E and HupB dynamics foster mycobacterial cell homeostasis and fitness. *iScience* **25**, 104233 (2022).

44. R. Priyadarshini, M. A. de Pedro, K. D. Young, Role of peptidoglycan amidases in the development and morphology of the division septum in Escherichia coli. *J Bacteriol* **189**, 5334-5347 (2007).

45. C. Heidrich *et al.*, Involvement of N-acetylmuramyl-L-alanine amidases in cell separation and antibiotic-induced autolysis of Escherichia coli. *Mol Microbiol* **41**, 167-178 (2001).

46. D. Mengin-Lecreulx, L. Texier, M. Rousseau, J. van Heijenoort, The murG gene of Escherichia coli codes for the UDP-N-acetylglucosamine: N-acetylmuramyl-(pentapeptide) pyrophosphoryl-undecaprenol N-acetylglucosamine transferase involved in the membrane steps of peptidoglycan synthesis. *J Bacteriol* **173**, 4625-4636 (1991).

47. A. H. Freeman *et al.*, Arginine methylation sites on SepIVA help balance elongation and septation in Mycobacterium smegmatis. *Mol Microbiol* **119**, 208-223 (2023).

48. J. Zhu *et al.*, Spatiotemporal localization of proteins in mycobacteria. *Cell Rep* **37**, 110154 (2021).

49. Z. He, J. De Buck, Cell wall proteome analysis of Mycobacterium smegmatis strain MC2 155. *BMC Microbiol* **10**, 121 (2010).

50. K. Choukate, B. Chaudhuri, Structural basis of self-assembly in the lipid-binding domain of mycobacterial polar growth factor Wag31. *IUCrJ* **7**, 767-776 (2020).

51. M. A. Oliva *et al.*, Features critical for membrane binding revealed by DivIVA crystal structure. *Embo j* **29**, 1988-2001 (2010).

52. L. D. Renner, D. B. Weibel, Cardiolipin microdomains localize to negatively curved regions of Escherichia coli membranes. *Proc Natl Acad Sci U S A* **108**, 6264-6269 (2011).

53. P. M. Oliver *et al.*, Localization of anionic phospholipids in Escherichia coli cells. *J Bacteriol* **196**, 3386-3398 (2014).

54. M. I. Garcia Fernandez, D. Ceccarelli, U. Muscatello, Use of the fluorescent dye 10-N-nonyl acridine orange in quantitative and location assays of cardiolipin: a study on different experimental models. *Anal Biochem* **328**, 174-180 (2004).

55. E. Mileykovskaya, W. Dowhan, Visualization of phospholipid domains in Escherichia coli by using the cardiolipin-specific fluorescent dye 10-N-nonyl acridine orange. *J Bacteriol* **182**, 1172-1175 (2000).

56. J. M. Petit, A. Maftah, M. H. Ratinaud, R. Julien, 10N-nonyl acridine orange interacts with cardiolipin and allows the quantification of this phospholipid in isolated mitochondria. *Eur J Biochem* **209**, 267-273 (1992).

57. C. Carel *et al.*, Mycobacterium tuberculosis proteins involved in mycolic acid synthesis and transport localize dynamically to the old growing pole and septum. *PLoS One* **9**, e97148 (2014).

58. N. H. Arejan, D. R. Czapski, J. A. Buonomo, C. C. Boutte, MmpL3, Wag31 and PlrA are involved in coordinating polar growth with peptidoglycan metabolism and nutrient availability. *bioRxiv* 10.1101/2024.04.29.591792 (2024).

59. G. P. Salmond, J. F. Lutkenhaus, W. D. Donachie, Identification of new genes in a cell envelope-cell division gene cluster of Escherichia coli: cell envelope gene murG. *J Bacteriol* **144**, 438-440 (1980).

60. R. Lenarcic *et al.*, Localisation of DivIVA by targeting to negatively curved membranes. *Embo j* **28**, 2272-2282 (2009).

61. G. Carranza *et al.*, Cardiolipin plays an essential role in the formation of intracellular membranes in Escherichia coli. *Biochim Biophys Acta Biomembr* **1859**, 1124-1132 (2017).

62. V. A. Gold *et al.*, The action of cardiolipin on the bacterial translocon. *Proc Natl Acad Sci U S A* **107**, 10044-10049 (2010).

63. W. S. Yeo, S. Dyzenhaus, V. J. Torres, S. R. Brinsmade, T. Bae, Regulation of Bacterial Two-Component Systems by Cardiolipin. *Infect Immun* **91**, e0004623 (2023).

64. S. P. Ouellette *et al.*, Localized cardiolipin synthesis is required for the assembly of MreB during the polarized cell division of Chlamydia trachomatis. *PLoS Pathog* **18**, e1010836 (2022).

65. J. C. van Kessel, G. F. Hatfull, Recombineering in Mycobacterium tuberculosis. *Nat Methods* **4**, 147-152 (2007).

66. A. Parikh *et al.*, Development of a new generation of vectors for gene expression, gene replacement, and protein-protein interaction studies in mycobacteria. *Appl Environ Microbiol* **79**, 1718-1729 (2013).

67. G. P. Jose, S. Gopan, S. Bhattacharyya, T. J. Pucadyil, A facile, sensitive and quantitative membrane-binding assay for proteins. *Traffic* **21**, 297-305 (2020).

68. J. Schindelin *et al.*, Fiji: an open-source platform for biological-image analysis. *Nat Methods* **9**, 676-682 (2012).

69. H. Schägger, Tricine-SDS-PAGE. *Nat Protoc* **1**, 16-22 (2006).

70. A. Kapopoulou, J. M. Lew, S. T. Cole, The MycoBrowser portal: a comprehensive and manually annotated resource for mycobacterial genomes. *Tuberculosis (Edinb)* **91**, 8-13 (2011).

71. K. Tunyasuvunakool *et al.*, Highly accurate protein structure prediction for the human proteome. *Nature* **596**, 590-596 (2021).

Figure 1

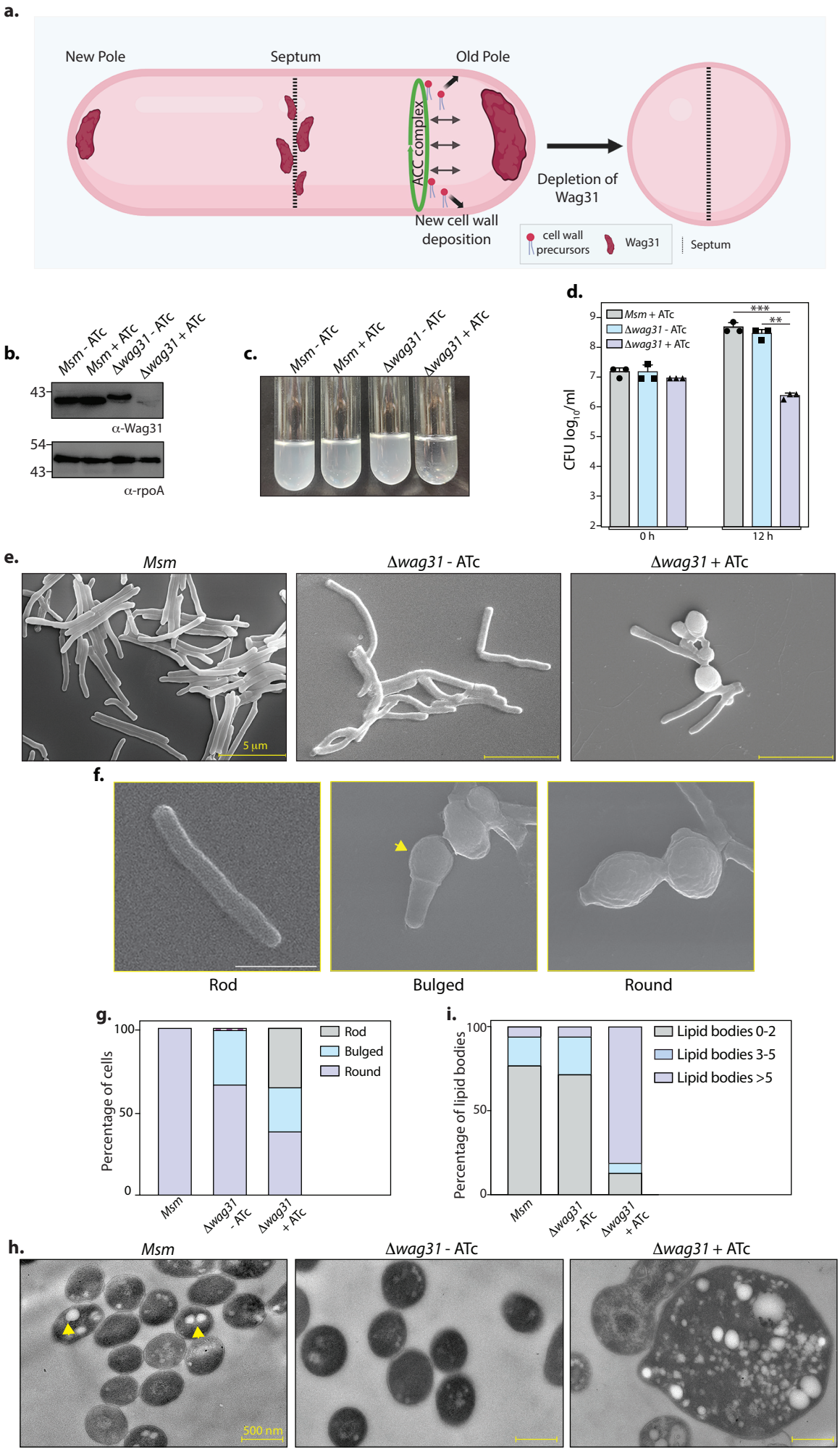
a.
New Pole
Septum
Old Pole
ACC complex
New cell wall deposition
Depletion of Wag31
cell wall precursors
Wag31
Septum
b.
Msm - ATc
Msm + ATc
Δwag31 - ATc
Δwag31 + ATc
43
α-Wag31
54
43
α-rpoA
c.
Msm - ATc
Msm + ATc
Δwag31 - ATc
Δwag31 + ATc
d.
Msm + ATc
Δwag31 - ATc
Δwag31 + ATc
CFU log10/ml
0 h
12 h
***
**
e.
Msm
Δwag31 - ATc
Δwag31 + ATc
5 µm
f.
Rod
Bulged
Round
g.
Percentage of cells
Rod
Bulged
Round
Msm
Δwag31 - ATc
Δwag31 + ATc
i.
Percentage of lipid bodies
Lipid bodies 0-2
Lipid bodies 3-5
Lipid bodies >5
Msm
Δwag31 - ATc
Δwag31 + ATc
h.
Msm
Δwag31 - ATc
Δwag31 + ATc
500 nm

Figure 2

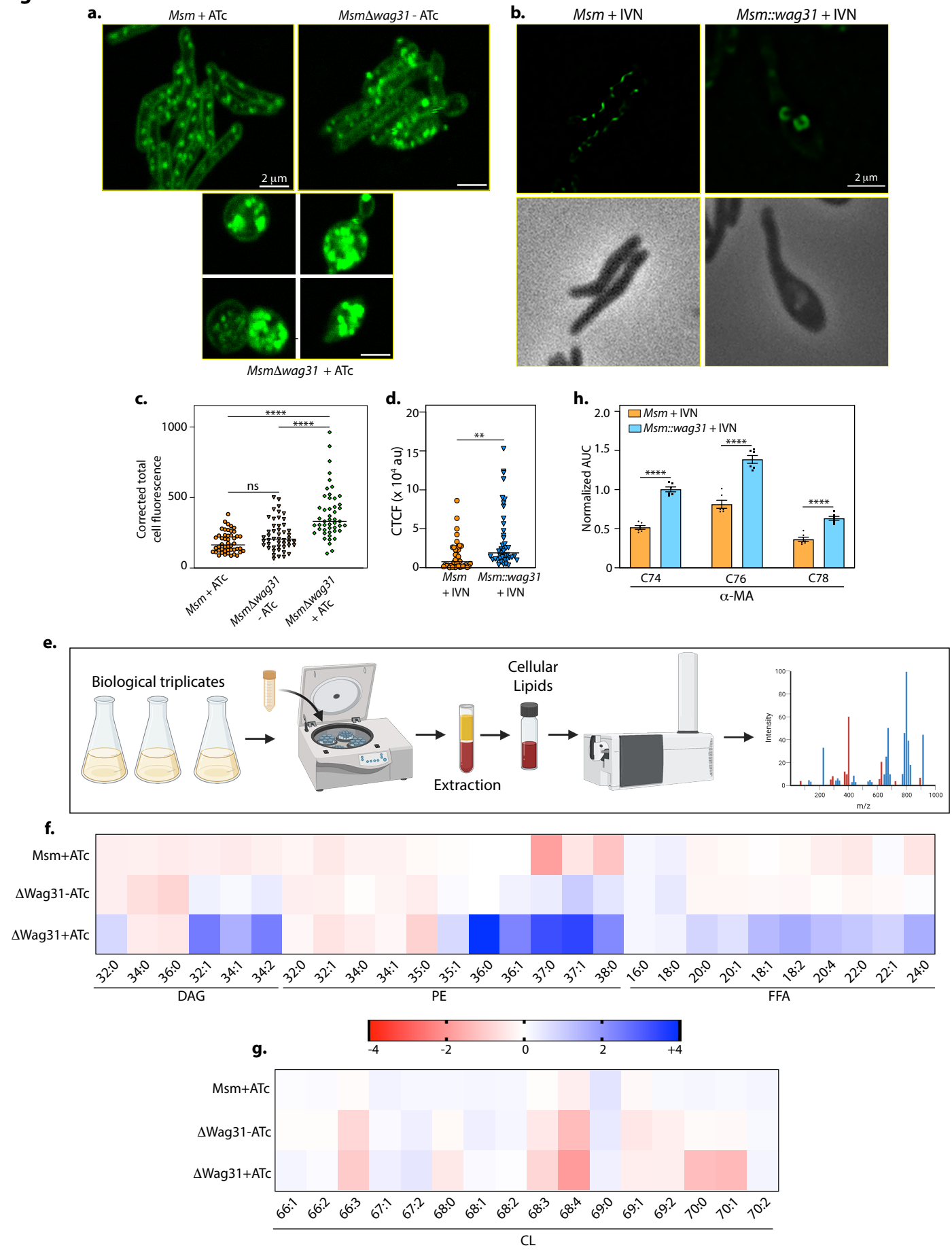
a.
Msm + ATc
MsmΔwag31 - ATc
2 µm
MsmΔwag31 + ATc
b.
Msm + IVN
Msm::wag31 + IVN
2 µm
c.
Corrected total cell fluorescence
1000
500
0
****
****
ns
Msm + ATc
MsmΔwag31 - ATc
MsmΔwag31 + ATc
d.
CTCF (x 10⁴ au)
20
15
10
5
0
**
Msm + IVN
Msm::wag31 + IVN
h.
Msm + IVN
Msm::wag31 + IVN
Normalized AUC
2.0
1.5
1.0
0.5
0
****
****
****
C74
C76
C78
α-MA
e.
Biological triplicates
Cellular Lipids
Extraction
Intensity
m/z
f.
Msm+ATc
ΔWag31-ATc
ΔWag31+ATc
32:0
34:0
36:0
32:1
34:1
34:2
32:0
32:1
34:0
34:1
35:0
35:1
36:0
36:1
37:0
37:1
38:0
16:0
18:0
20:0
20:1
18:1
18:2
20:4
22:0
22:1
24:0
DAG
PE
FFA
-4
-2
0
2
+4
g.
Msm+ATc
ΔWag31-ATc
ΔWag31+ATc
66:1
66:2
66:3
67:1
67:2
68:0
68:1
68:2
68:3
68:4
69:0
69:1
69:2
70:0
70:1
70:2
CL

Figure 3

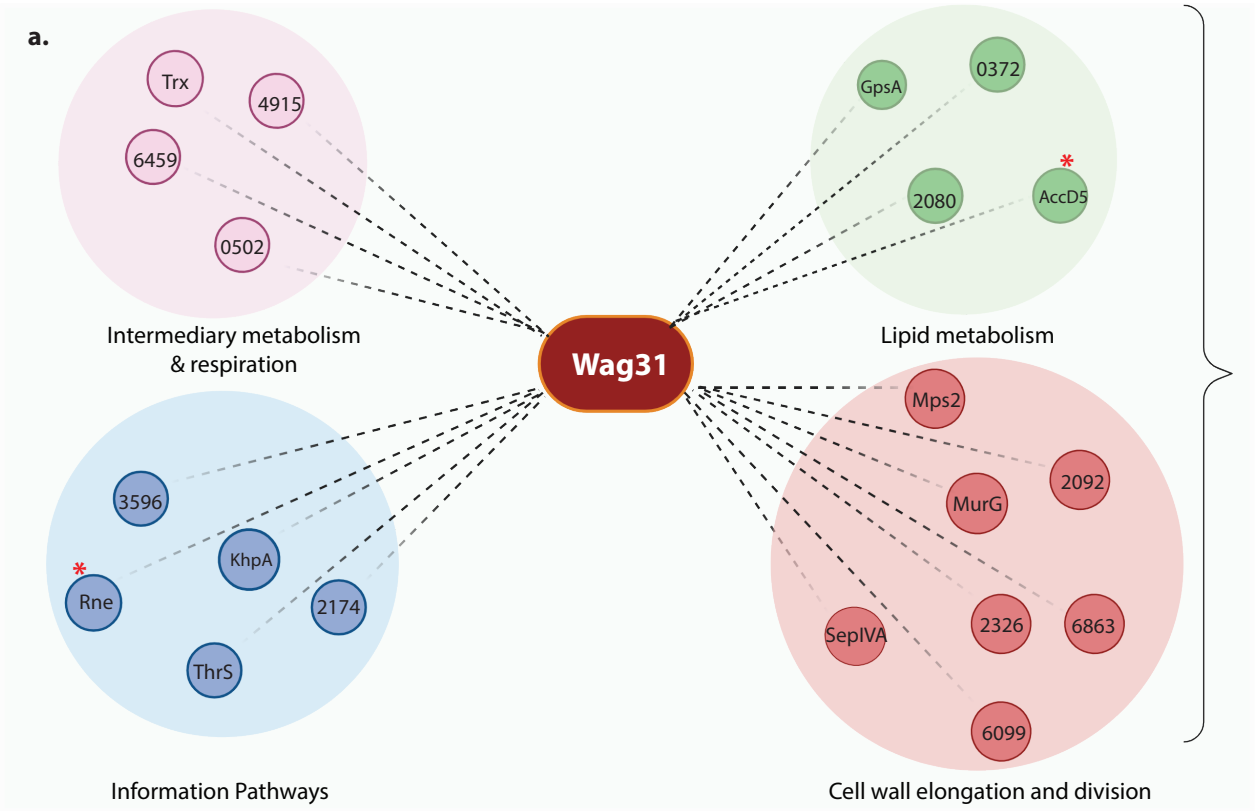
a.
Trx
4915
6459
0502
Intermediary metabolism & respiration
GpsA
0372
2080
AccD5
Lipid metabolism
Wag31
3596
KhpA
Rne
2174
ThrS
Information Pathways
Mps2
2092
MurG
SepIVA
2326
6863
6099
Cell wall elongation and division

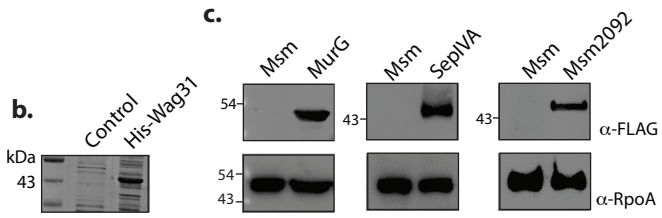
b.
Control
His-Wag31
kDa
43
c.
Msm
MurG
Msm
SepIVA
Msm
Msm2092
54
43
α-FLAG
α-RpoA

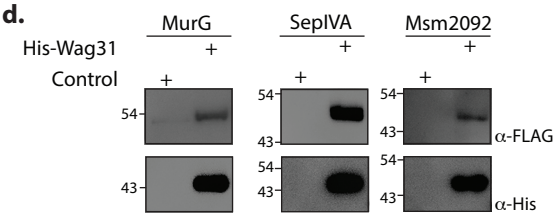
d.
His-Wag31
Control
MurG
SepIVA
Msm2092
+
54
43
α-FLAG
α-His

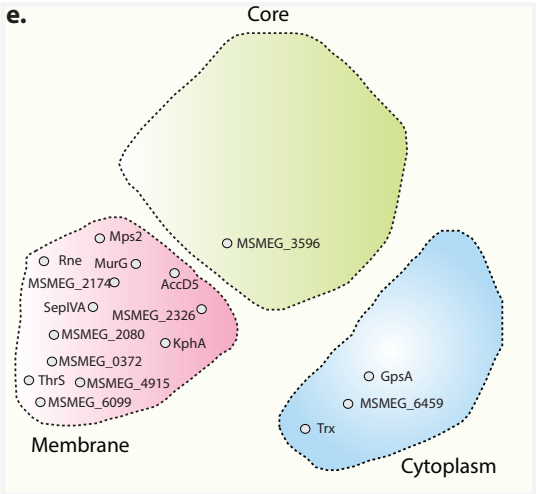
e.
Core
MSMEG_3596
Mps2
Rne
MurG
MSMEG_2174
AccD5
SepIVA
MSMEG_2326
MSMEG_2080
KphA
MSMEG_0372
ThrS
MSMEG_4915
MSMEG_6099
Membrane
GpsA
MSMEG_6459
Trx
Cytoplasm

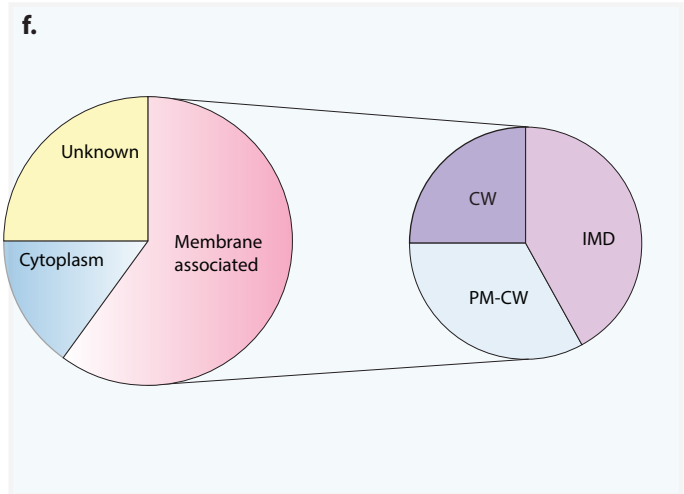
f.
Unknown
Membrane associated
Cytoplasm
CW
IMD
PM-CW

Figure 4

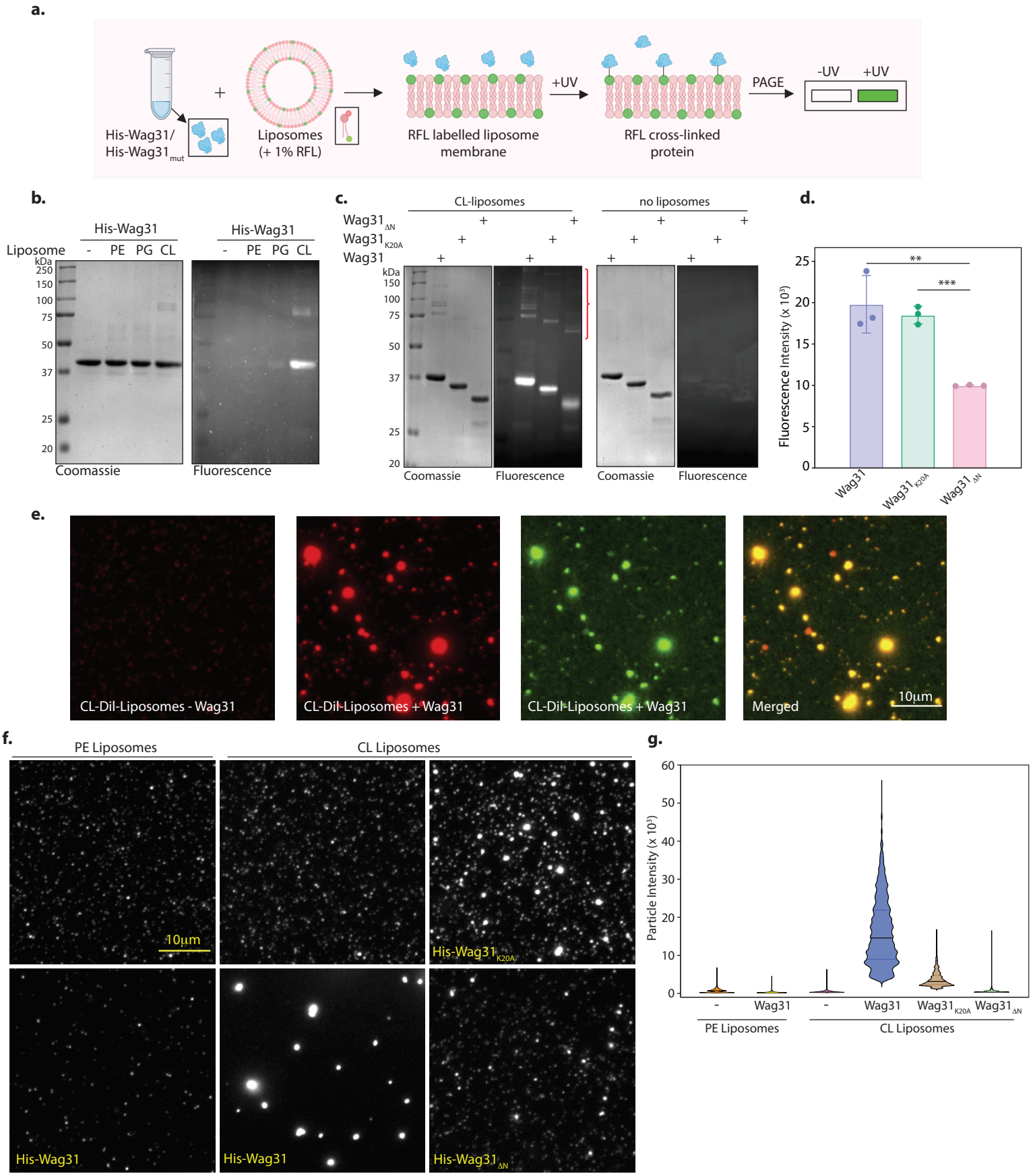
a.
His-Wag31/
His-Wag31mut
Liposomes
(+ 1% RFL)
RFL labelled liposome
membrane
+UV
RFL cross-linked
protein
PAGE
-UV
+UV
b.
His-Wag31
Liposome
- PE PG CL
kDa
250
150
100
75
50
37
25
20
Coomassie
Fluorescence
c.
CL-liposomes
no liposomes
Wag31ΔN
Wag31K20A
Wag31
Coomassie
Fluorescence
d.
Fluorescence Intensity (x 10³)
**
***
Wag31
Wag31K20A
Wag31ΔN
e.
CL-Dil-Liposomes - Wag31
CL-Dil-Liposomes + Wag31
CL-Dil-Liposomes + Wag31
Merged
10µm
f.
PE Liposomes
CL Liposomes
10µm
His-Wag31K20A
His-Wag31
His-Wag31
His-Wag31ΔN
g.
Particle Intensity (x 10³)
-
Wag31
-
Wag31
Wag31K20A
Wag31ΔN
PE Liposomes
CL Liposomes

Figure 5

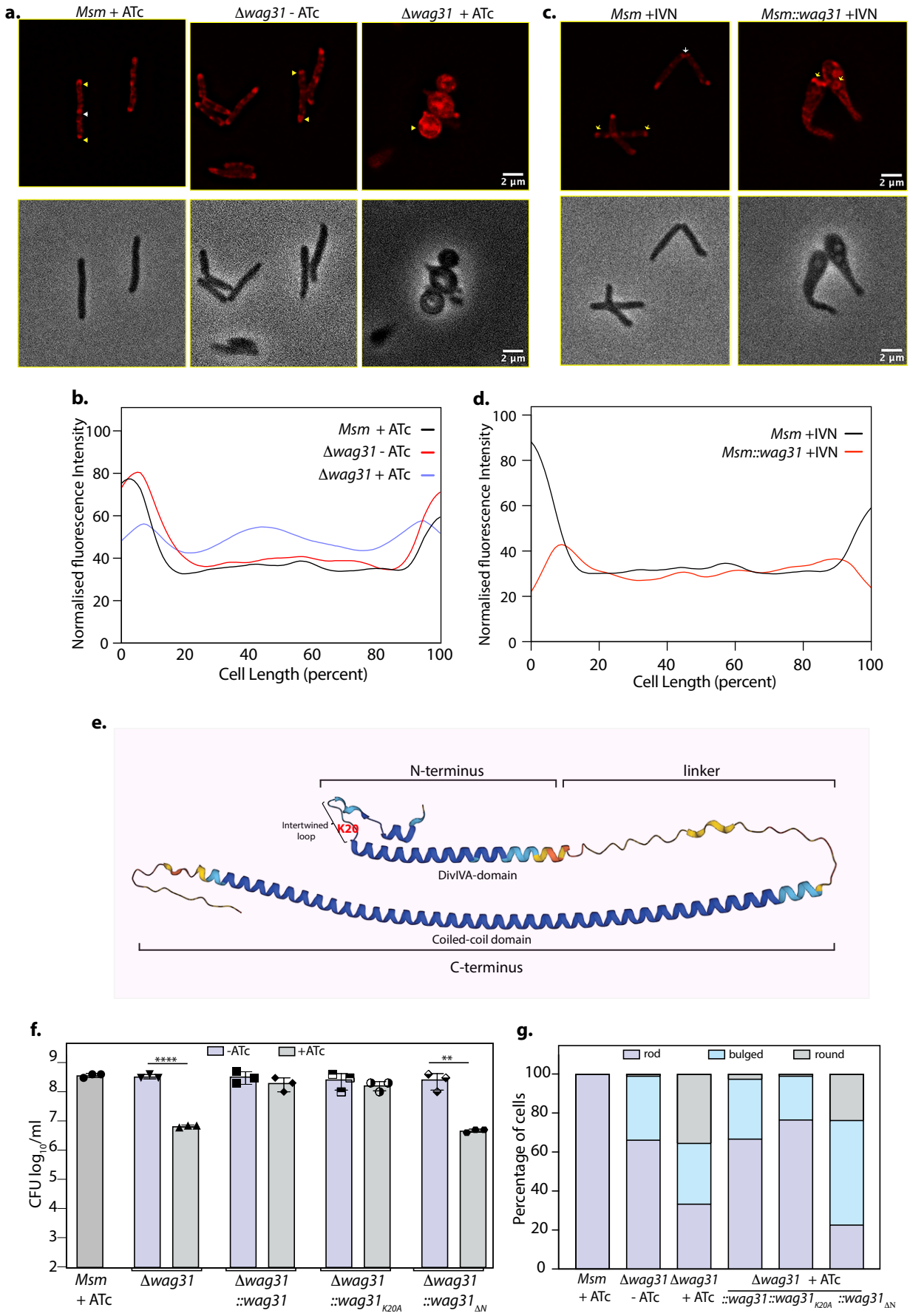
a.
Msm + ATc
Δwag31 - ATc
Δwag31 + ATc
2 µm
c.
Msm +IVN
Msm::wag31 +IVN
2 µm
b.
Normalised fluorescence Intensity
Msm + ATc
Δwag31 - ATc
Δwag31 + ATc
Cell Length (percent)
d.
Normalised fluorescence Intensity
Msm +IVN
Msm::wag31 +IVN
Cell Length (percent)
e.
N-terminus
linker
Intertwined loop
K20
DivIVA-domain
Coiled-coil domain
C-terminus
f.
-ATc
+ATc
****
**
CFU log10/ml
Msm + ATc
Δwag31
Δwag31 ::wag31
Δwag31 ::wag31K20A
Δwag31 ::wag31ΔN
g.
rod
bulged
round
Percentage of cells
Msm + ATc
Δwag31 - ATc
Δwag31 + ATc
Δwag31 + ATc
::wag31
::wag31K20A
::wag31ΔN

Figure 6

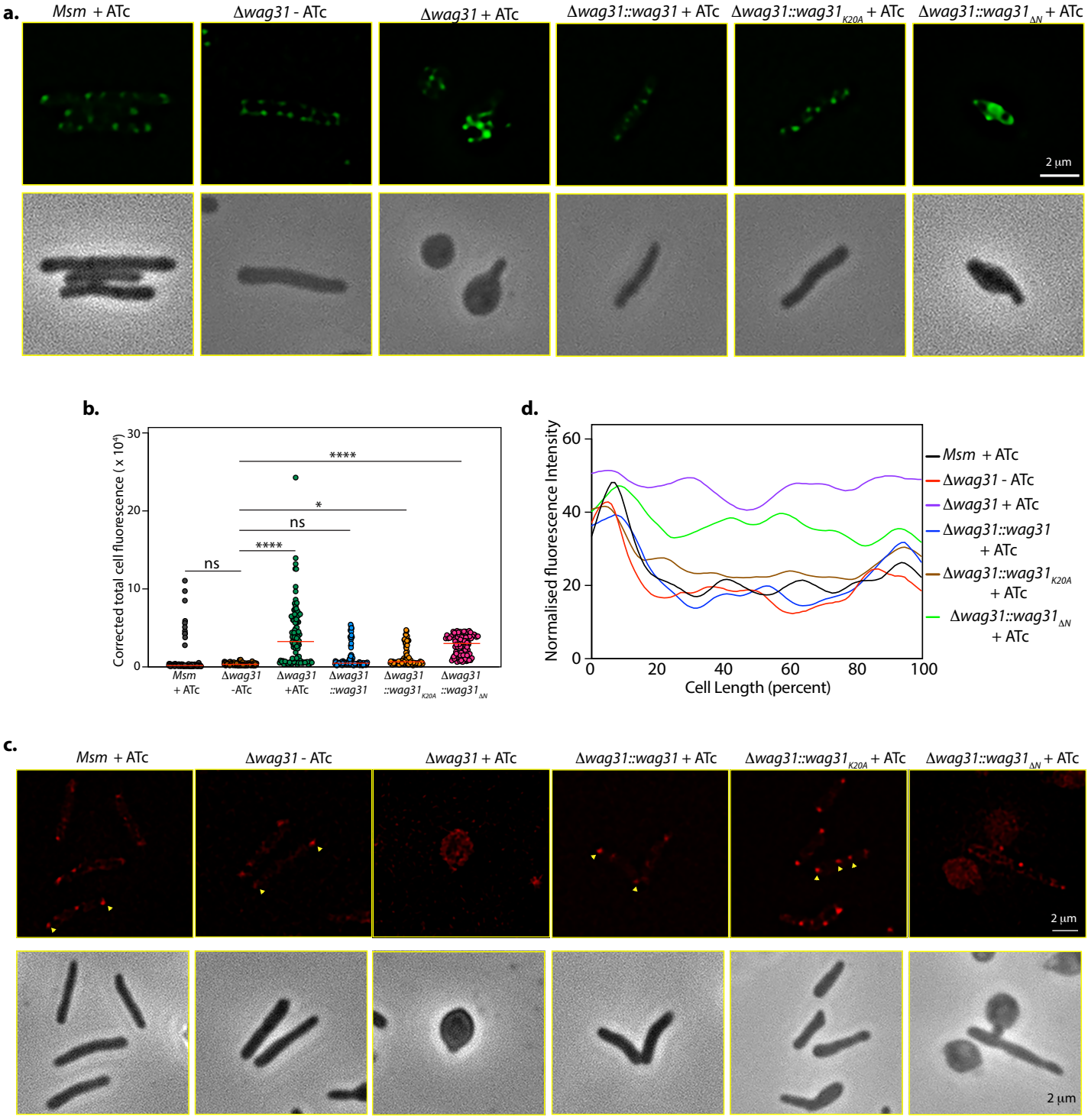
a.
Msm + ATc
Δwag31 - ATc
Δwag31 + ATc
Δwag31::wag31 + ATc
Δwag31::wag31K20A + ATc
Δwag31::wag31ΔN + ATc
2 µm
b.
Corrected total cell fluorescence (x 10⁴)
30
20
10
0
****
*
ns
****
ns
Msm + ATc
Δwag31 -ATc
Δwag31 +ATc
Δwag31 ::wag31
Δwag31 ::wag31K20A
Δwag31 ::wag31ΔN
d.
Normalised fluorescence Intensity
60
40
20
0
0
20
40
60
80
100
Cell Length (percent)
Msm + ATc
Δwag31 - ATc
Δwag31 + ATc
Δwag31::wag31 + ATc
Δwag31::wag31K20A + ATc
Δwag31::wag31ΔN + ATc
c.
Msm + ATc
Δwag31 - ATc
Δwag31 + ATc
Δwag31::wag31 + ATc
Δwag31::wag31K20A + ATc
Δwag31::wag31ΔN + ATc
2 µm
2 µm

Figure7

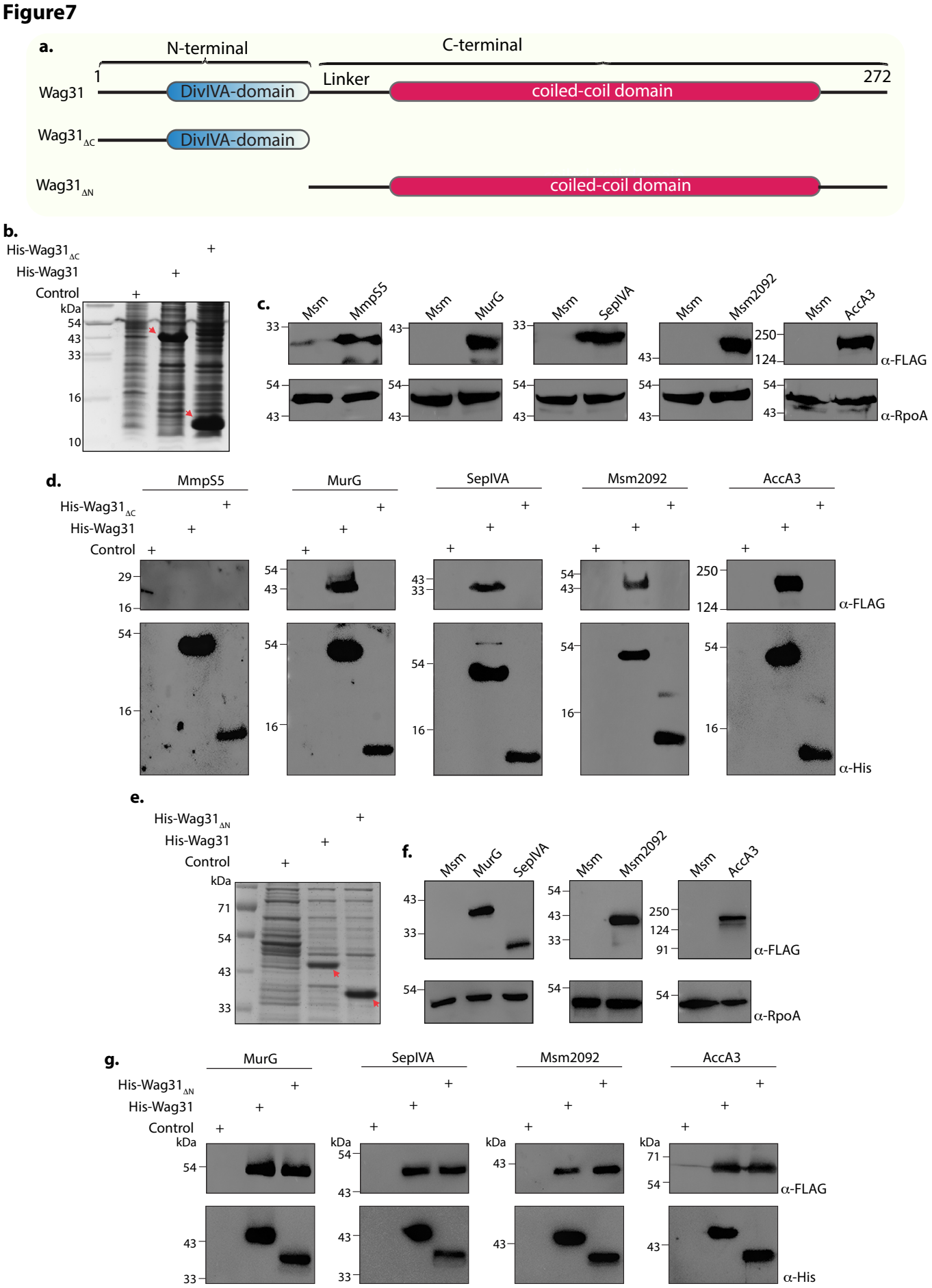
a.
N-terminal
C-terminal
1
272
Linker
Wag31
DivIVA-domain
coiled-coil domain
Wag31ΔC
DivIVA-domain
Wag31ΔN
coiled-coil domain
b.
His-Wag31ΔC
His-Wag31
Control
kDa
54
43
33
16
10
c.
Msm
MmpS5
MurG
SepIVA
Msm2092
AccA3
α-FLAG
α-RpoA
d.
MmpS5
MurG
SepIVA
Msm2092
AccA3
His-Wag31ΔC
His-Wag31
Control
α-FLAG
α-His
e.
His-Wag31ΔN
His-Wag31
Control
kDa
71
54
43
33
f.
Msm
MurG
SepIVA
Msm2092
AccA3
α-FLAG
α-RpoA
g.
MurG
SepIVA
Msm2092
AccA3
His-Wag31ΔN
His-Wag31
Control
kDa
α-FLAG
α-His

Figure 8

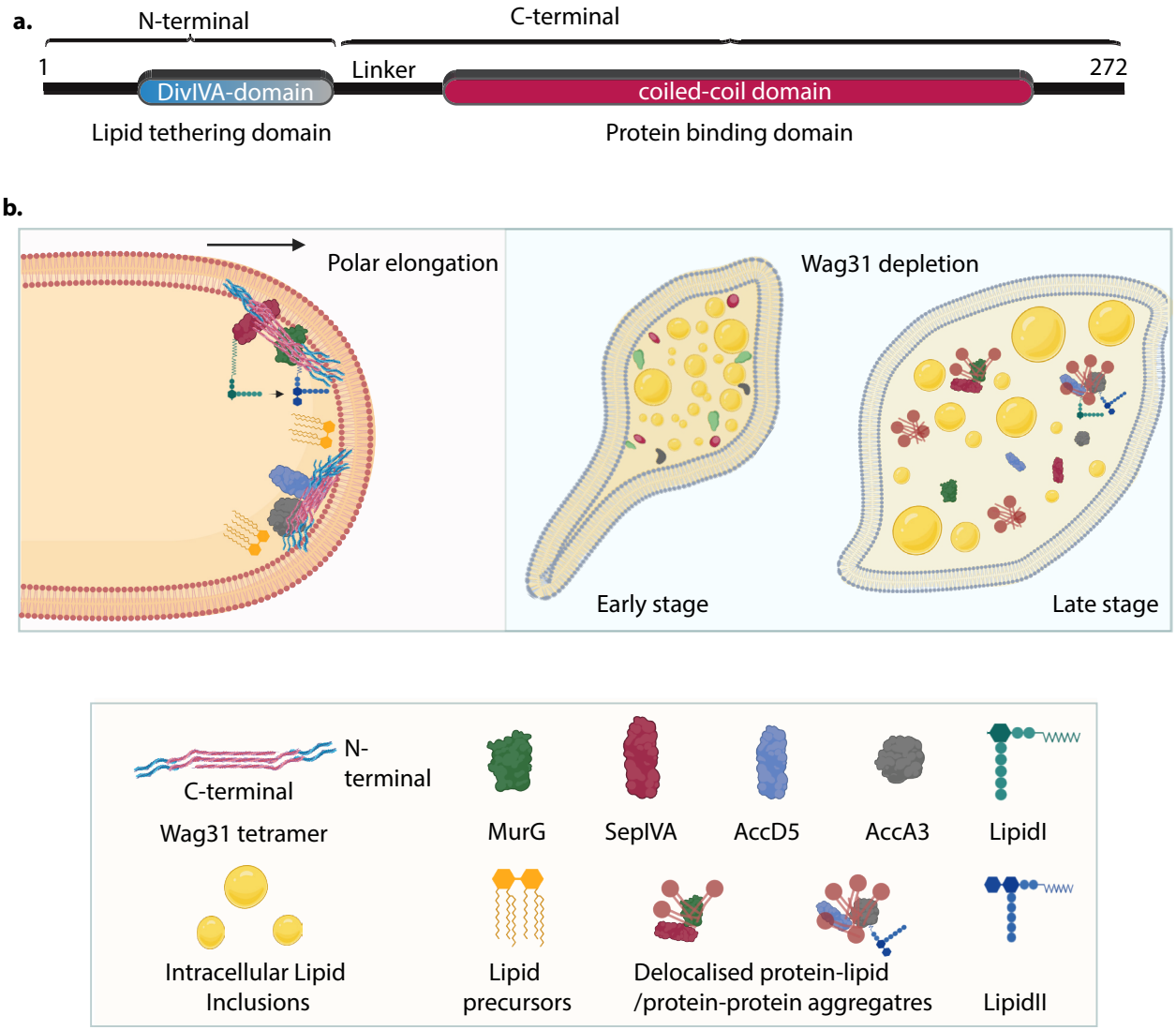
a.
N-terminal
C-terminal
1
Linker
272
DivIVA-domain
coiled-coil domain
Lipid tethering domain
Protein binding domain
b.
Polar elongation
Wag31 depletion
Early stage
Late stage
N-terminal
C-terminal
Wag31 tetramer
MurG
SepIVA
AccD5
AccA3
LipidI
Intracellular Lipid Inclusions
Lipid precursors
Delocalised protein-lipid /protein-protein aggregatres
LipidII

Figure S1

a.

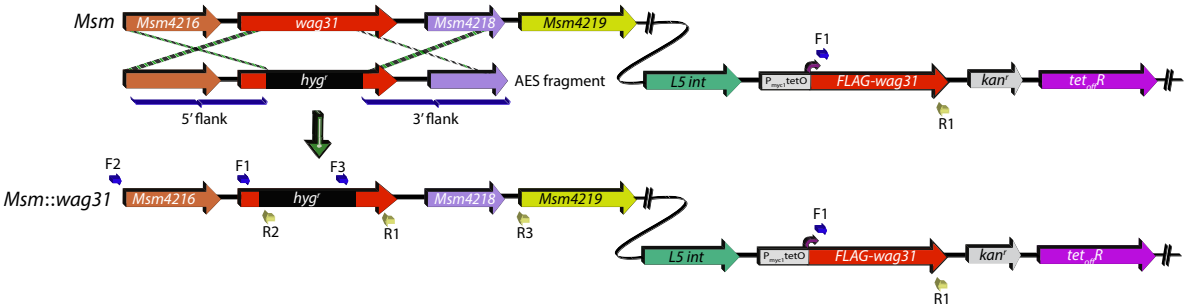
Msm
Msm4216
wag31
Msm4218
Msm4219
hyg'
AES fragment
5' flank
3' flank
L5 int
FLAG-wag31
kan'
F1
R1
Msm::wag31
F2
F3
R2
R3

b.

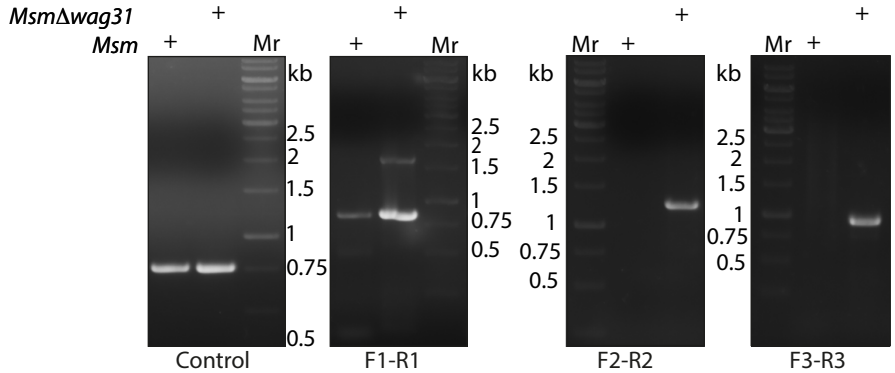
MsmΔwag31
Msm
+
Mr
kb
2.5
2
1.5
1
0.75
0.5
Control
F1-R1
F2-R2
F3-R3

Figure S2

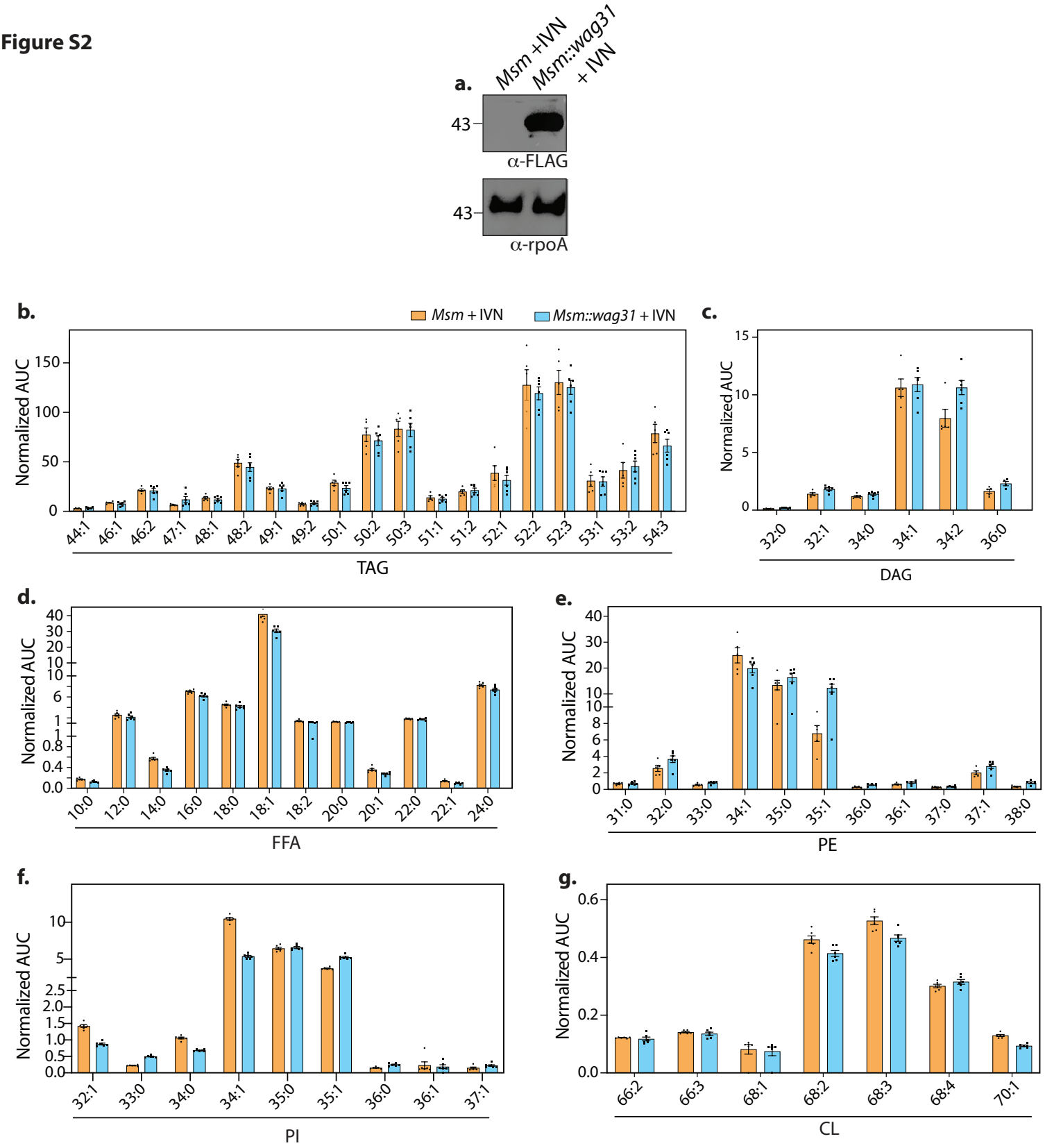
a.
Msm +IVN
Msm::wag31 + IVN
43
α-FLAG
43
α-rpoA
b.
Msm + IVN
Msm::wag31 + IVN
Normalized AUC
44:1
46:1
46:2
47:1
48:1
48:2
49:1
49:2
50:1
50:2
50:3
51:1
51:2
52:1
52:2
52:3
53:1
53:2
54:3
TAG
c.
Normalized AUC
32:0
32:1
34:0
34:1
34:2
36:0
DAG
d.
Normalized AUC
10:0
12:0
14:0
16:0
18:0
18:1
18:2
20:0
20:1
22:0
22:1
24:0
FFA
e.
Normalized AUC
31:0
32:0
33:0
34:1
35:0
35:1
36:0
36:1
37:0
37:1
38:0
PE
f.
Normalized AUC
32:1
33:0
34:0
34:1
35:0
35:1
36:0
36:1
37:1
PI
g.
Normalized AUC
66:2
66:3
68:1
68:2
68:3
68:4
70:1
CL

Figure S3

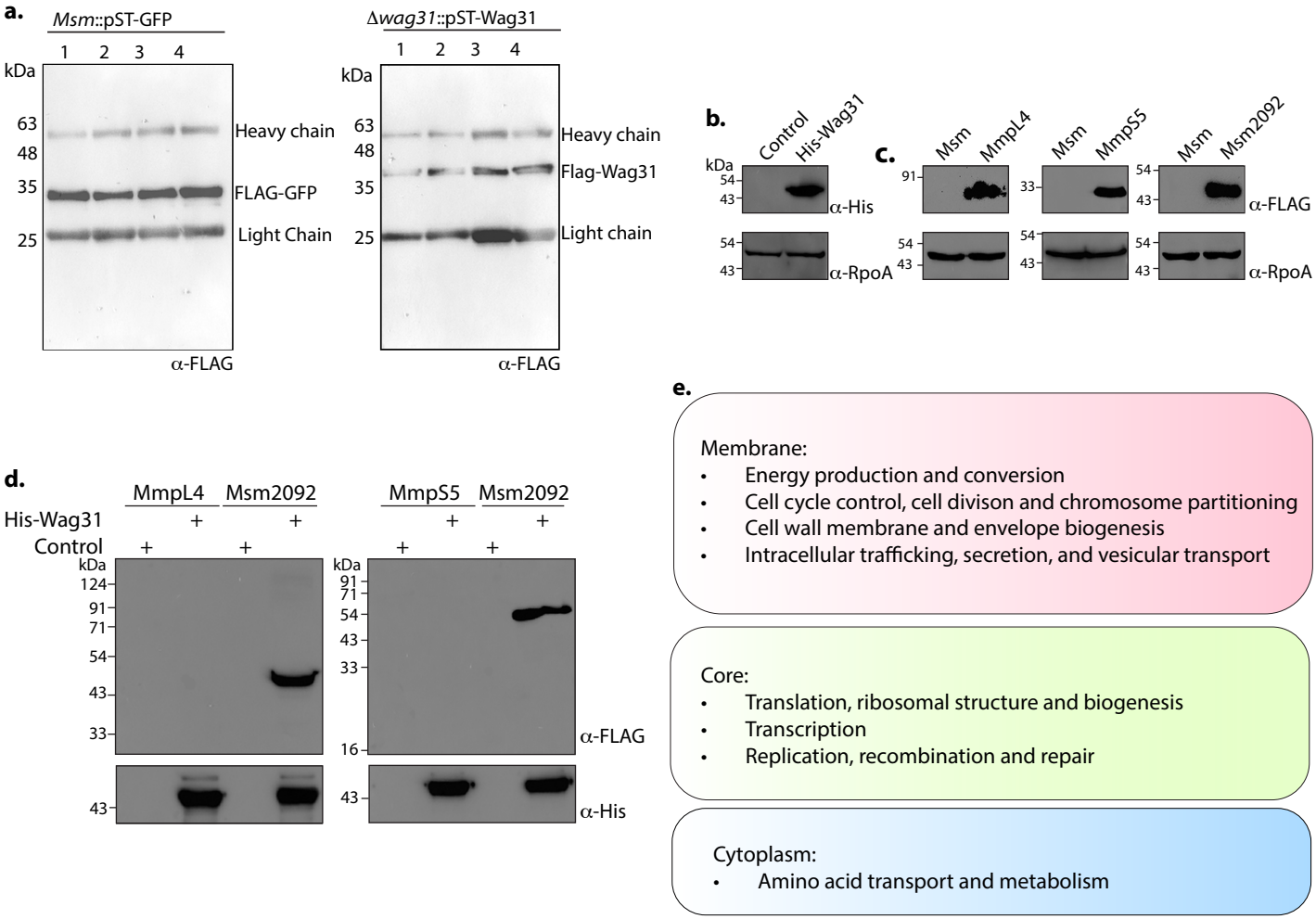
a.
Msm::pST-GFP
1 2 3 4
kDa
63
48
35
25
Heavy chain
FLAG-GFP
Light Chain
α-FLAG
Δwag31::pST-Wag31
1 2 3 4
kDa
63
48
35
25
Heavy chain
Flag-Wag31
Light chain
α-FLAG
b.
Control
His-Wag31
kDa
54
43
α-His
54
43
α-RpoA
c.
Msm
MmpL4
Msm
MmpS5
Msm
Msm2092
91
33
54
43
α-FLAG
54
43
54
43
54
43
α-RpoA
d.
MmpL4
Msm2092
MmpS5
Msm2092
His-Wag31
Control
kDa
124
91
71
54
43
33
43
kDa
91
71
54
43
33
16
43
α-FLAG
α-His
e.
Membrane:
• Energy production and conversion
• Cell cycle control, cell divison and chromosome partitioning
• Cell wall membrane and envelope biogenesis
• Intracellular trafficking, secretion, and vesicular transport
Core:
• Translation, ribosomal structure and biogenesis
• Transcription
• Replication, recombination and repair
Cytoplasm:
• Amino acid transport and metabolism

Figure S4

Cell wall & cell processes

- MSMEG_0402/mps2: linear gramicidin synthetase subunit D
- MSMEG_6099: conserved transmembrane protein
- MSMEG_4227: murG: undecaprenyldiphospho-muramoylpentapeptide beta-N-acetylglucosaminyltransferase
- MSMEG_2092: D-aminopeptidase
- MSMEG_6863: class II aldolase/adducin domain protein
- MSMEG_2416: SepIVA: DivIVA-domain containing protein
- MSMEG_1046: ABC-type molybdenum transport system
- MSMEG_0386: NAD dependent epimerase/dehydratase family protein
- MSMEG_3654: ATPase SecA2
- MSMEG_4958: diaminopimelate decarboxylase
- MSMEG_0919: heparin-binding hemagglutinin
- MSMEG_1954: ABC1 family protein
- MSMEG_2326: ABC-type molybdenum transport system

Lipid metabolism

- MSMEG_1813: propionyl-CoA carboxylase beta chain
- MSMEG_0372: oxidoreductase, short chain dehydrogenase/ reductase family protein
- MSMEG_2393: NAD-dependent glycerol-3-phosphate dehydrogenase
- MSMEG_2080: putative acyl-CoA dehydrogenase
- MSMEG_0912: 3-hydroxybutyryl-CoA dehydrogenase
- MSMEG_2648: Sfp-type phosphopantetheinyl transferase
- MSMEG_0406: fadE5: acyl-coA-dehydrogenase
- MSMEG_5199: putative acyl-CoA dehydrogenase
- MSMEG_4709: enoyl-CoA hydratase
- MSMEG_5197: long-chain specific acyl-CoA dehydrogenase
- MSMEG_6512: acyl-CoA dehydrogenase domain protein
- MSMEG_6511: acyl-CoA dehydrogenase domain protein
- MSMEG_6208: palmitoyl-CoA hydrolase
- MSMEG_5198: carnitinyl-CoA dehydratase

Replication, recombination & repair

- MSMEG_3596: ATPase- DNA replication
- MSMEG_2174: superfamily protein I DNA or RNA helicase
- MSMEG_1061: phosphohydrolase
- MSMEG_2768: OB-fold nucleic acid binding domain protein
- MSMEG_4450: alpha/beta hydrolase
- MSMEG_1930: DEAD/DEAH box helicase
- MSMEG_5156: base excision DNA repair protein, HhH-GPD family protein

Translation, ribosome structure & biogenesis

- MSMEG_4626: rne: ribonuclease, Rne/Rng family protein
- MSMEG_2931: thrS: threonyl-tRNA synthetase
- MSMEG_3003: aspS: aspartyl-tRNA synthetase
- MSMEG_4959: argS: arginyl-tRNA synthetase
- MSMEG_3777: pheT: phenylalanyl-tRNA synthetase, beta subunit

Regulatory proteins

- MSMEG_6219: moxR2: ATPase family protein associated with various cellular activities (AAA)
- MSMEG_4659: GntR-family protein transcriptional regulator
- MSMEG_3363: regulatory protein, TetR
- MSMEG_0035: fhaA: FHA domain protein

Unknown

- MSMEG_3785: PfkB-family protein carbohydrate kinase
- MSMEG_6783: integral membrane protein
- MSMEG_4652: D-oliose 4-ketoreductase
- MSMEG_1679: AmiB

Miscellaneous

- MSMEG_6514: trehalose synthase-fused probable maltokinase

Intermediary metabolism & respiration

- MSMEG_4915: alpha-glucan phosphorylase family protein
- MSMEG_0502: glucosidase
- MSMEG_6459: ferredoxin-dependent glutamate synthase 1
- MSMEG_3138: trx: thioredoxin
- MSMEG_0594: iron-sulfur cluster binding protein
- MSMEG_5427:prs: ribose-phosphate pyrophosphokinase
- MSMEG_2611: pyridine nucleotide-disulphide oxidoreductase family protein
- MSMEG_5937: bphl-2: 4-hydroxy-2-oxovalerate aldolase
- MSMEG_3051: gmk: guanylate kinase
- MSMEG_3044: pyrC: dihydroorotase
- MSMEG_1037: adhc1: alcohol dehydrogenase, zinc-containing
- MSMEG_4294: glnA: glutamine synthetase, type I
- MSMEG_3632: gnd: 6-phosphogluconate dehydrogenase, decarboxylating
- MSMEG_3100: opcA: OpcA protein: Putative OXPP cycle protein OpcA
- MSMEG_3894: prcA: proteasome alpha subunit
- MSMEG_2379: leuB: 3-isopropylmalate dehydrogenase
- MSMEG_6874: aldehyde dehydrogenase
- MSMEG_6114: ppa: inorganic pyrophosphatase
- MSMEG_1073: oxidoreductase, short-chain dehydrogenase/reductase family protein
- MSMEG_1825: rmlD: dTDP-4-dehydrorhamnose reductase
- MSMEG_3746: pyrG: CTP synthase
- MSMEG_4272: HesB/YadR/YfhF family protein
- MSMEG_3451: short-chain dehydrogenase/reductase, NAD(P)H-binding
- MSMEG_5592: Luciferase like monooxygenase
- MSMEG_0220; monoglyceride lipase
- MSMEG_3880: nitrilase/cyanide hydratase and apolipoprotein N-acyltransferase
- MSMEG_5903: oxidoreductase, short chain dehydrogenase/reductase family protein
- MSMEG_0759: purA: CTP synthase
- MSMEG_6598: ribH: 6,7-dimethyl-8-ribityllumazine synthase
- MSMEG_6351: histidinol-phosphate aminotransferase
- MSMEG_4528: cysH: phosphoadenosine phosphosulfate reductase
- MSMEG_4276: ilvE: branched-chain amino acid aminotransferase
- MSMEG_1670: sdhA: succinate dehydrogenase, flavoprotein subunit
- MSMEG_0539: transcriptional regulator, Crp/Fnr family protein
- MSMEG_4258: trpD: anthranilate phosphoribosyltransferase
- MSMEG_2357: cysteine desulfurase
- MSMEG_3207: hisB: imidazoleglycerol-phosphate dehydratase
- cobyrinic Acid a,c-diamide synthase
- alpha oxoglutarate ferredoxin oxidoreductase, beta subunit
- short chain dehydrogenase
- fructose-1,6-bisphosphatase, class II
- MSMEG_2617: cobB: cobyrinic Acid a,c-diamide synthase
- MSMEG_4645: orB: alpha oxoglutarate ferredoxin oxidoreductase, beta subunit
- MSMEG_3619: short chain dehydrogenase
- MSMEG_5239: glpX: fructose-1,6-bisphosphatase, class II
- MSMEG_3071: ribE: riboflavin synthase, alpha subunit
- MSMEG_0793: thiG: thiazole biosynthesis protein
- MSMEG_0956: hemB: delta-aminolevulinic acid dehydratase
- MSMEG_3219: indole-3-glycerol phosphate synthase
- MSMEG_0239: O-acetylhomoserine/O-acetylserine sulfhydrylase
- MSMEG_5515: purH: bifunctional purine biosynthesis protein
- MSMEG_6256: asd: aspartate-semialdehyde dehydrogenase

Amino acid transport and metabolism

- MSMEG_5211: aminotransferase class-III

Conserved hypotheticals

- MSMEG_2436; MSMEG_0897
- MSMEG_6941; MSMEG_3309
- MSMEG_2481; MSMEG_2434
- MSMEG_3148; MSMEG_6901
- MSMEG_6499; MSMEG_1340
- MSMEG_1514; MSMEG_5691
- MSMEG_3942; MSMEG_4282
- MSMEG_1049; MSMEG_3024
- MSMEG_3244; MSMEG_0240
- MSMEG_2685; MSMEG_4193
- MSMEG_2329

Membrane

Cytoplasm

Core